Interface Modification and Characterization of Nanostructured Semiconductors

A Bridge to Contemporary Electronics

Irish, Austin

2024

Citation for published version (APA):
Irish, A. (2024). *Interface Modification and Characterization of Nanostructured Semiconductors: A Bridge to Contemporary Electronics*. [Doctoral Thesis (compilation), Lund University]. Lund University.

Total number of authors:
1

LUND UNIVERSITY

PO Box 117
221 00 Lund
+46 46-222 00 00

Interface Modification and Characterization of Nanostructured Semiconductors

A Bridge to Contemporary Electronics

AUSTIN IRISH

DEPARTMENT OF PHYSICS | FACULTY OF SCIENCE | LUND UNIVERSITY

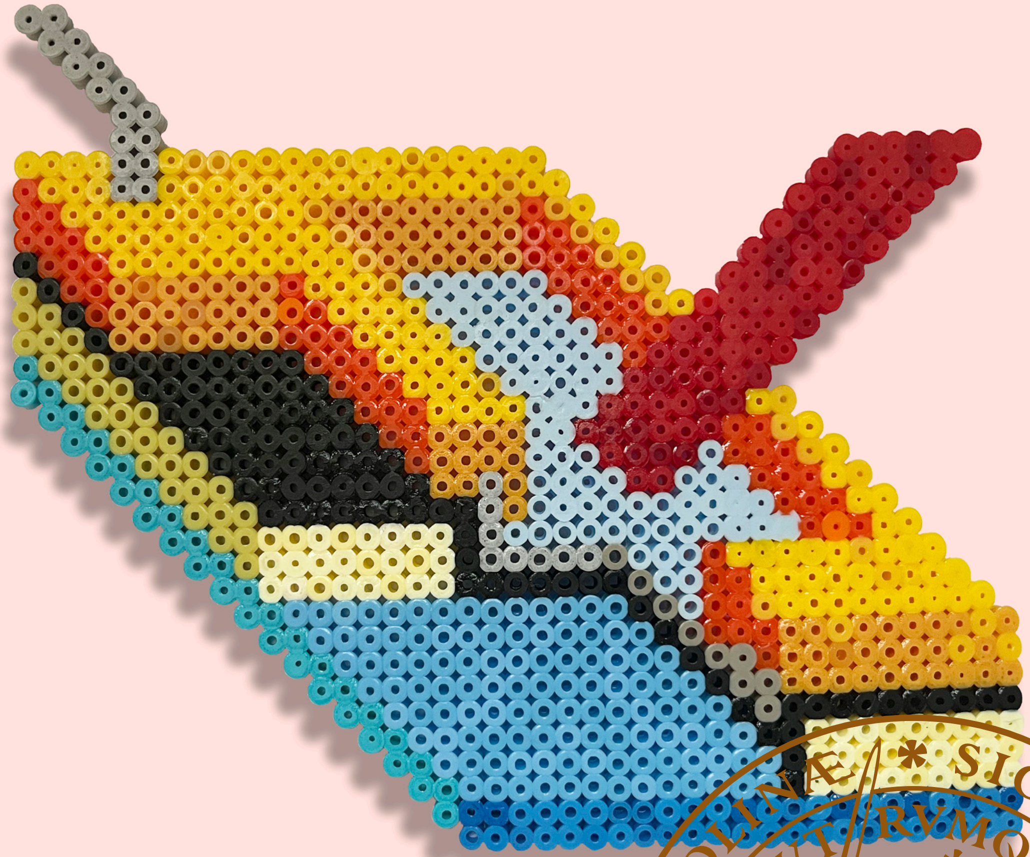

Interface Modification and Characterization of Nanostructured Semiconductors

A Bridge to Contemporary Electronics

Austin Irish

DOCTORAL DISSERTATION

Doctoral dissertation for the degree of Doctor of Philosophy (PhD) at the Faculty of Science at Lund University to be publicly defended on the 18th of October, 2024 at 13.15 in the Rydberg Lecture Hall, Department of Physics, Sölvegatan 14, Lund, Sweden.

Faculty opponent
Prof. Christopher Hinkle, University of Notre Dame

Organization: LUND UNIVERSITY

Document name: Doctoral Thesis

Date of issue 2024-10-18

Author(s): Austin Irish

Sponsoring organization:

Title and subtitle: Interface Modification and Characterization of Nanostructured Semiconductors:

A Bridge to Contemporary Electronics

Abstract:

This research presents advancements into the fabrication, operation and characterization of electronic nanomaterials and devices. It focuses on the interfaces of metals, oxides and semiconductors and developing techniques to improve their integration into devices. Covering nanoelectronics from photovoltaics to circuit elements, a combined suite of scanning probe and X-ray techniques was used to provide insight into structural and electronic properties.

Scanning probe techniques such as piezoresponse force microscopy corroborated the formation of ultrathin ferroelectric hafnia films. A unique Kelvin probe force microscopy method for nondestructively measuring directly on nanowire arrays complemented electron beam induced current in the investigation of photovoltaic p-n junctions. Temperature- and time-dependent photoluminescence spectroscopy was used show how nitrogen plasma treatment could increase GaAs nanowire solar cell efficiency, while photoelectron spectroscopy demonstrated surface conversion to GaN and long-term passivation.

X-ray radiation from synchrotrons such as MAX IV enabled the probing of novel circuit components. X-ray absorption spectroscopy helped to explain reactive sputtering of TiN, connecting electrode texturing with device endurance and remanent polarization. Photoemission spectroscopy was integral to understanding the impact of device fabrication on thin film behavior. For resistive random-access memory, it controverted conventional wisdom by showing that interlayer oxidation protected key device functionality. In ferroelectric devices it proved the opposite, highlighting the necessity for short timescale thermal processes to limit film decomposition. Finally, operando hard X-ray photoelectron spectroscopy was employed to follow ferroelectric switching in real time. Synchrotron compatible devices were developed, and characterization of buried interfaces revealed a polarization dependent, reversible redox between HZO and InAs which, if left unchecked, ultimately leads to breakdown.

Generally, this work confirms that, independent of the specific material and device application, it is crucial to have a large characterization toolbox at hand, especially one that includes surface-sensitive techniques tailored for operando measurements at the micro- and nanoscale.

Key words:

Classification system and/or index terms (if any)

Supplementary bibliographical information

Language: English

ISSN and key title:

ISBN:

978-91-8039-980-7 (print)

978-91-8039-981-4 (electronic)

Recipient's notes

Number of pages: 50

Price

Security classification

I, the undersigned, being the copyright owner of the abstract of the above-mentioned dissertation, hereby grant to all reference sources permission to publish and disseminate the abstract of the above-mentioned dissertation.

Signature

Date 2024-09-06

Interface Modification and Characterization of Nanostructured Semiconductors

A Bridge to Contemporary Electronics

Austin Irish

LUND
UNIVERSITY

Coverphotos by Inda Brinkmann and Zephyr Rosenblod

Faculty of Science
Department of Physics

ISBN 978-91-8039-980-7 (print)
ISBN 978-91-8039-981-4 (electronic)

Printed in Sweden by Media-Tryck, Lund University
Lund 2024

NORDIC SWAN ECOLABEL
Printed matter
3041 0903

Media-Tryck is a Nordic Swan Ecolabel
certified provider of printed material.
Read more about our environmental
work at www.mediatryck.lu.se
MADE IN SWEDEN

Table of Contents

Acknowledgments

My recent years at Lund University, and especially those at the Synchrotron Radiation Research Division, have been characterized by tremendous fun, challenges, growth and change. It still surprises me how universally the positive attitude, generous spirit, and passion for knowledge permeates nearly every student, researcher and professor in this small city. I wish for nothing more than that this would continue to radiate out and brighten our occasionally tumultuous world.

At the center of this, I would like to thank my supervisor, Rainer Timm who sets an impeccable example of personal and professional excellence. His dedication to his work is only paralleled by that to his family and community. He is an inspiration, a pleasure to work with, and indefatigable; an unfair role model. No matter how organized I was, no matter how deep I got into literature, no matter how busy he was, he always found time to give helpful, incisive feedback and critical guidance. I can't imagine succeeding without his support.

I owe a great deal to several other professors. Magnus Borgström and Arkady Yartsev provided an early foundation that proved critical to the development of my scientific skills and interests. Their persistence has made me what I am today. Lars-Erik Wernersson and Mattias Borg have been irreplaceable sources of interesting and fruitful collaboration. Their drive for excellence in research is delightful and infectious. Anders Mikkelsen, Joachim Schnadt and Edvin Lundgren provided the background support, oversight and inspiration that is vital to PhD student success yet seldom recognized. I am very grateful.

Mathieu Gisselbrecht, I still think you were wrong about my master's thesis; thank you for your unexpectedly playful yet intense life discussions. To Stacey Sörensen, Ian McNulty, and Jason Beech, thank you for giving me both professional and rock climbing inspiration.

A small army of PhD and post-doc peers gave me the bulk of my education, entertainment and emotional support: Ahmed, Alfred, André, Andrea, Anton, Auden, Benjamin, David, Dmitry, Enrique, Foqia, Giulio, Hanna, Hannes, Nelia, Nishant, Lukas, Maria, Robin, Rohit, Rosemary, Saketh, Sandra, Ulrike, Vidar, Virginia, Xianshao, Yen-Po, Yi and honestly, so so many more.

Thank you for the laughter.

Peace,

Zephyr

Popular Science Summary

Considering the discovery of electrons is barely a century old, the speed and ubiquity with which electrical devices have reshaped the globe is astonishing. From lightbulbs and telegraphs to computers, LEDs and renewable energy, it is hard to think of modern society without a solar panel or a mobile phone. The success of electricity is due to the small size and tremendous speed with which energy and signals can be transmitted. As humans and technology have expanded, the need and desire for advancements have pushed these technologies to impressive extremes. Though having one's telephone-camera-computer fall out of a pocket seems like a real risk today, the first computers of the twentieth century occupied the space of an entire studio apartment. It can be difficult to comprehend. Modern transistors have now shrunk eighteen orders of magnitude and their components can be measured in atomic thicknesses. A nanometer is one billionth of a meter. To put this in perspective, the width of a billion human hairs is about 100 km or the width of Skåne (or more importantly, the train ride from my favorite place to climb, Kjugekull, to my favorite beach, Ribersborgstranden). Whereas developing the next generation of computers or solar cells offers unprecedented opportunities, studying these complex materials at the nanoscale presents many new challenges. The work done in this thesis was dedicated to creating novel nanostructures and developing techniques to measure and improve them. To this end, synchrotron and cleanroom laboratories such as MAX IV and the Lund Nanolab were essential. Synchrotrons produce enough X-rays to see even the smallest materials, materials of such cleanliness and precision that cleanroom entrance is forbidden to those wearing fragrances or who have recently smoked. On studies of light collecting nanowires made of GaAs, a new technique was developed to clean and preserve their surfaces for higher efficiency. This involved reacting hydrogen with oxygen on their surface to create and then remove water, and using nitrogen plasma to encase the nanowires in a protective shell. On similar InP nanowires, a unique atomic force microscopy setup was developed as a way to measure these light collecting arrays in situ, providing authentic feedback on the electrical quality of their surfaces in the same conditions as they are built. Ultra-thin films containing hafnium oxide were also studied for the purpose of creating improved logic and memory devices for computers. Single nanowire devices were shown capable of combining previously separate systems of the computer, demonstrating potential improvements to both size and speed. Here, synchrotron experiments were able to show how subtle changes to the way oxygen is added to insulators can literally make or break these devices. Heating hafnium oxide and doping it with zirconium, to give it an additional functionality called ferroelectricity, was also a major theme of research. Since many electronic materials are temperature sensitive, faster, localized laser annealing techniques were explored to keep industrial compatibility. Here, X-ray techniques such as photoelectron and absorption spectroscopy were used to describe how metal-oxide-semiconductor interfaces deteriorate and useful procedures recommended. Finally, *operando* spectroscopy was used to show how these devices function and change in real time, tracking the movement and reactivity of atoms within their layers. As a whole, this research highlights how state-of-the-art laboratories can provide insight into some of the smallest objects humans can create. Developing these techniques helps us understand how nanoelectronics work and lays a foundation as we leap into the next generation of devices.

List of Papers

In this thesis the following papers are included.

Paper I

Athle, R., Persson, A. E., Irish, A., Menon, H., Timm, R., & Borg, M. (2021). Effects of TiN top electrode texturing on ferroelectricity in $Hf_xZr_{1-x}O_2$. ACS Applied Materials & Interfaces, 13(9), 11089-11095.

For the XAS and PES components, I planned and performed the experiment, analyzed the results, produced the figures and wrote the corresponding text.

Paper II

Ram, M. S., Persson, K. M., Irish, A., Jönsson, A., Timm, R., & Wernersson, L. E. (2021). High-density logic-in-memory devices using vertical indium arsenide nanowires on silicon. Nature Electronics, 4(12), 914-920.

For the PES components, I performed the experiment, analyzed the results, produced the figures and wrote the corresponding text.

Paper III

Athle, R., Blom, T., Irish, A., Persson, A. E., Wernersson, L. E., Timm, R., & Borg, M. (2022). Improved endurance of ferroelectric $Hf_xZr_{1-x}O_2$ integrated on InAs using millisecond annealing. Advanced Materials Interfaces, 9(27), 2201038.

For the PES components, I performed the experiment, analyzed the results, produced the figures and wrote the corresponding text.

Paper IV

Irish, A., Zou, X., Barrigon, E., D'Acunto, G., Timm, R., Borgström, M. T., & Yartsev, A. (2023). Nitrogen plasma passivation of GaAs nanowires resolved by temperature dependent photoluminescence. Nano Express, 3(4), 045008.

I conceived the idea and planned and performed the experiments. I made samples, analyzed the results, produced the figures and wrote the text.

Paper V

Robin Athle, Megan O Hill, Austin Irish, Huaiyu Chen, Rainer Timm, Elias Kristensson, Jesper Wallentin and Mattias Borg (2024). Ferroelectricity in Ultra-thin HfO_2-based Films by Nanosecond Laser Annealing (Manuscript in review)

For the PES components, I performed the experiment, analyzed the results, produced the figures and wrote the corresponding text.

Paper VI

Austin Irish, Anton E. O. Persson, André Andersen, Vidar Flodgren, Andrea Troian, Yen-Po Liu, Lars-Erik Wernersson, Rainer Timm (2024). Switching Dynamics and Interface Chemistry of Ferroelectric Hafnia Devices (Manuscript)

For the PES components, I got the beamtime, planned and performed the experiments, analyzed the results and produced the figures. I was the main responsible for writing the text.

Paper VII

Austin Irish, Lukas Hrachowina, David Alcer, Magnus Borgström, Rainer Timm (2024). On the Edge: *In situ* Kelvin Probe AFM on InP Nanowire Arrays (Manuscript)

I conceived the idea, planned and performed the experiment, analyzed the results, produced the figures and wrote the text.

The following papers are not included in this thesis.

Paper VIII

Lucas A. B. Marçal, Sandra Benter, Austin Irish, Dmitry Dzhigaev, Eitan Oksenberg, Amnon Rothman, Ella Sanders, Susanna Hammarberg, Zhaojun Zhang, Simone Sala, Alexander Björling, Eva Unger, Anders Mikkelsen, Ernesto Joselevich, Rainer Timm, and Jesper Wallentin (2021) Inducing ferroelastic domains in single-crystal $CsPbBr_3$ perovskite nanowires using atomic force microscopy. Physical Review Materials 5 L063001

Paper IX

S. Benter , Y. Liu , R. D. P. Maciel , C. S. Ong , L. Linnala , D. Pan , A. Irish , Y.-P. Liu , J. Zhao , H. Xu , O. Eriksson , R. Timm , and A. Mikkelsen , Tuneable 2D surface Bismuth incorporation on InAs nanosheets. Nanoscale 15, 9551 (2023).

Paper X

Liu, Y.; Benter, S.; Ong, C. S.; Maciel, R. P.; Bjork, L.; Irish, A.; Eriksson, O.; Mikkelsen, A.; Timm, R. A 2D Bismuth-Induced Honeycomb Surface Structure on GaAs(111). ACS Nano 2023, 17, 5047– 5058

Abbreviations

AFM	Atomic Force Microscopy
ALD	Atomic Layer Deposition
BE	Binding Energy
CB	Conduction Band
CVD	Chemical Vapor Deposition
EBIC	Electron Beam Induced Current
EXAFS	Extended X-Ray Absorption Fine Structure
FE	Ferroelectricity
FET	Field Effect Transistor
FLA	Flash Lamp Annealing
FTJ	Ferroelectric Tunnel Junction
FWHM	Hull Width at Half Maximum
HAXPES	Hard X-ray Photoelectron Spectroscopy
HZO	$Hf_xZr_{1-x}O_2$
IMFP	Inelastic Mean Free Path
KE	Kinetic Energy
NEXAFS	Near Edge X-Ray Absorption Fine Structure
NLA	Nanosecond Laser Annealing
KPFM	Kelvin Probe Force Microscopy
NEXAFS	Near Edge X-ray Absorption Fine Structure
NW	Nanowire
MOS	Metal Oxide Semiconductor
MOVPE	Metalorganic Vapor-phase Epitaxy
PFM	Piezoresponse Force Microscopy
PL	Photoluminescence
PES	Photoelectron Spectroscopy
PUND	Positive Up Negative Down
PVD	Physical Vapor Deposition

ReRAM	Resistive Random-Access Memory
RTP	Rapid Thermal Processing
SEM	Scanning Electron Microscopy
SMU	Source Measure Unit
SPM	Scanning Probe Microscopy
STM	Scanning Tunneling Microscopy
TRPL	Time Resolved Photoluminescence
VB	Valence Band
XANES	X-ray Absorption Near Edge Structure
XAS	X-ray Absorption Spectroscopy
XPS	X-ray Photoelectron Spectroscopy (see PES)

1 Introduction

The twenty-first century has been marked by a surge of big data and hunger for energy. Bitcoin mining consumes as much electricity as Sweden[1,2]. The large language models sweeping the globe such as GPT require supercomputers to train on trillions of words for a period of months[3]. Whether it's work or recreation, cloud data storage and processing permeate everything from Google Workspace to Netflix. As demand increases, pressure to develop new technologies pushes research into previously unexplored directions. Intel founder Gordon Moore famously observed the doubling of computer transistors annually. Though exponential growth persisted for decades, we are now reaching the fundamental limits of our physical systems and the conventional ways of building and using them.

As the distance between computer transistors is now only tens of molecules, scaling through shrinkage is no longer an option. In fact, neither is simply creating larger integrated circuits. Because of the tremendous advancements made in memory size and processing speed, the limiting factor in computation is now the transfer of data between the two. This bottleneck is intrinsic to the Von Neumann architecture and comes from the physical separation of the memory from the processor. In-memory computing is an exciting alternative which integrates logic and memory, eliminating communication time and naturally lending itself to new technologies like neuromorphic computing. So, to continuously achieve faster, smaller and more energy efficient electronics, their design must be radically reconsidered.

Nevertheless, arrangement is far from the only consideration. Choices in material, form and fabrication also play a large role. In this thesis, III-V materials were incorporated into in-memory structures and other advanced devices as they are semiconductors which offer tunable properties and extreme flexibility. InAs, for example, has high electron mobility and is excellent for high-speed electronics applications. GaAs and InP, on the other hand, have a direct bandgap near the theoretical maximum for efficient light absorption making them excellent for solar cells. Here, structuring these materials into nanowires has played an important role. Because of their reduced footprint, in photovoltaics, arrays of nanowires allow flexible, efficient films to be produced with a fraction of the material and cost. In computer electronics, the nanowire structure enabled the dense integration of both a transistor and a memristor into single devices with the theoretically minimum area.

In other cases, it is not form but function that plays a central role. Key to achieving enhanced functionality in devices is to imbue regular materials with new properties. In the development of memristive devices, hafnium oxide has been indispensable due to its ability to offer a high dielectric constant alongside programmable resistivity. In hafnia memories based on conductive filaments, tunable resistivity can be achieved via mobile defects such as oxygen vacancies. Large electric fields can induce a partial breakdown of the dielectric, changing conduction. The process is reversible, allowing the setting of distinct memory states. By co-locating this resistive memory element with a transistor in a single nanowire we demonstrated in-memory computation. Hafnia also has the ability to form and sustain a ferroelectric phase. Ferroelectricity, is a major topic of this thesis and has been studied for applications in field effect transistors, tunnel junctions and random-access memory. Its controllable and persisting electric polarization is exploited in such memristor designs which promise high endurance and low-power consumption. Obtaining ferroelectricity in hafnium oxides can be achieved through strain engineering, where doping and annealing at high temperatures creates an energetically favorable phase transformation. This was obtained by sandwiching nanometer thin films between two metals which have different lattice constants and thermal expansion coefficients.

Creating these structures, understanding their functioning, and increasing their technological readiness is not without challenges, however. Volume scales with length cubed, while area does to its square. A three monolayer film has twice as many molecules on its surface than in the bulk. As electronics approach the atomic scale, surface phenomena begin to dominate and even the smallest imperfections become more costly. In nanowire solar cells, even perfect III-V crystals undergo oxidation in air and surface defect states interfere with the collection of electrons, hindering efficiency. In resistive memories, thin films have shown the potential to break down under electrical stress. In hafnia thin films, the ferroelectric phase transition occurs at several hundred degrees Celsius, making it incompatible with other fabrication processes. Having identified major problems within these fields, significant research was dedicated to understanding and developing methods to overcome these challenges. In particular, the MAX IV, Diamond and SOLEIL synchrotrons, and the Lund Nano Lab were essential.

Third generation synchrotrons produce high brilliance, tunable X-rays and provided the backbone of the materials characterization presented in this thesis. X-ray photoelectron (PES) and absorption spectroscopies (XAS) were used to probe through the first several nanometers of electronic material, revealing the composition and behavior of thin film deposition and interfacial reactions. **Paper I** employed XAS to describe the effect of molecular nitrogen on TiN deposition in ferroelectric capacitors. An important correlation was found connecting the metal film's growth direction, the oxide's remanent polarization and the lifespan of devices. PES was central to findings in **Papers II, III, V and VI**. In **Paper II** it was used to characterize the growth of hafnium oxide by plasma enhanced atomic layer deposition and explain why deliberate oxidation of the metal-oxide interface was necessary for resistive memory but not the transistors controlling them. **Papers III and V** took advantage of PES's chemical sensitivity to elucidate film degradation and defect creation, demonstrating how short laser pulses can be used to locally heat hafnium oxide at short timescales, protecting interfaces and sparing front end of line fabrication. **Paper VI** also looked at buried ferroelectric interfaces, but used synchrotron compatible devices and hard X-rays to probe even deeper. During these *operando* studies, metal-oxide redox was discovered which explained premature device failure and the importance of a clean interface. **Paper IV** used plasma nitridation to clean and protect photovoltaic nanowire surfaces. This work incorporated visible light into the characterization. Time resolved photoluminescence spectroscopy demonstrated defect passivation and X-ray photoelectron spectroscopy confirmed the permanent removal of surface oxide. Lastly, **Paper VII** looked at nanowire arrays for photovoltaics. A novel setup for atomic force microscopy was proposed as an alternative for non-destructive, topographical and electrical surface characterization. Though fully understanding this research and the solutions offered by it likely requires a comprehensive reading of literature, this text will provide an introduction to all of the major concepts and techniques employed to drive progress forward.

2 Characterization

2.1 X-rays

2.1.1 Interaction with matter

In 1901, the first Nobel Prize in physics was awarded for the discovery of X-rays[4]. German scientist Wilhelm Röntgen noted that this new type of light was unique in its weak interaction with matter. His serendipitous discovery was made during experiments with cathode rays (electron beams) where he expected fluorescence outside the vacuum tube but only along the axis of the beam, since the glass and cardboard enclosures were opaque to light and electrons. Surprisingly, before the experiment even began, his barium platinocyanide screen fluoresced despite not being in front of the beam. Quickly he realized that a new type of electromagnetic radiation existed, one with high energy that easily penetrated low density matter. After photographing transmission through his wife's hand revealed significant contrast between tissue (carbon), bone (calcium) and wedding ring (gold), the field of X-ray imaging was immediately born.

2.2 Spectroscopy

2.2.1 Photoelectron Spectroscopy

2.2.1.1 Introduction

Photoelectron spectroscopy (PES), also known as X-ray photoelectron spectroscopy (XPS), is an experimental technique dating back to observations made by German physicist Heinrich Hertz in the late 19th century, when electromagnetic radiation (i.e. photons) impinging on a metal coil was observed ejecting electrons and generating a current. This discovery became known as the photoelectric effect and led to two Nobel Prizes. The first was awarded to another famous German physicist, Albert Einstein, who in 1922 was recognized for his 1905 article "On a Heuristic Viewpoint Concerning the Production and Transformation of Light" in which he used the idea of "light quanta" (photons) to explain and formulize the photoelectric effect. The resulting conservation of energy equation has become fundamental in modern physics,

$$h\upsilon = \mathrm{KE} + \varphi\ , \qquad (2.2.1)$$

where KE is the kinetic energy of an electron, h is Planck's constant, υ is the frequency of the light, and φ is the work function of the material.

The photoelectric effect went on to found a major role in materials characterization thanks to Swedish physicist and 1981 Nobel laureate, Kai Siegbahn. In the 1950's Siegbahn pioneered the development of electron spectroscopy as a tool for chemical analysis, a technique which he coined ESCA. Since spectroscopy can be done for myriad reasons and photoelectrons can be generated by electromagnetic radiation generally, not just X-rays, this text will use the generalized term photoelectron spectroscopy to refer to all photon-in, photoelectron-out techniques. To understand PES, remarkably, we need little more than a definitional adjustment to equation (2.2.1). For research, excitation energy is controlled by the experimenter, kinetic energy is measured by an electron analyzer, and the focus becomes electron binding energy, which contains a wealth of information. The governing equation looks like:

$$KE = h\upsilon - \mathrm{BE} - \varphi_s + \varphi_a\ , \qquad (2.2.2)$$

where $h\upsilon$ is the excitation energy, and the binding energy of the photoelectron, BE, is defined relative to the Fermi level. The work function is the minimum energy needed to move an electron from the Fermi level of the sample/analyzer into vacuum just outside the material. Though elemental fingerprinting via measurement of electron kinetic energy is both practical and trivial, perhaps *the* major discovery of PES is chemical shifting.

Not only are the binding energies of electrons unique to their atomic and principal quantum numbers (e.g. O 1s), they can also shift due to local changes in potential like bonding and screening. Though III-V semiconductors and their oxides have bonds of a significant covalent nature, the redistribution of charge of valence electrons toward more negative anions often leads to changes in binding energy which are measurable by PES. In As_2O_3, for example, six arsenic valence electrons are given up to bonding with the oxygen atoms. This leads to core electrons more strongly bound to the arsenic nucleus and results in an increased binding energy. In Figure 2.2.1 we see a measurement done on nanowires grown for solar cells. After growth, even a perfect sample of GaAs will oxidize in ambient. This results in arsenic atoms in two different chemical states which produce clearly distinguishable signals. The binding energy of the native arsenic oxide observed here was 3.0 eV higher than that of bulk GaAs. In **Paper I** it was demonstrated that this material could not only be removed temporarily through HCl etching and H_2 plasma, but also prevented from returning via N_2 plasma passivation.

PES is often described as a surface sensitive technique. This is because unlike X-rays, for example, electrons interact strongly with matter. To understand the extent of this, it is useful to think about a concept known as inelastic mean free path

(IMFP). IMFP is a measure of how far an electron can travel through matter before losing energy and invalidating equation 2.2.2. This can be due to processes like absorption, but it is also affected by scattering. In fact, inelastic scattering of electrons with lower binding energy is what causes the background signal in PES. The intensity of electrons which have traveled a distance d without losing energy follows a Beer's Law-like exponential decay equation,

$$\mathrm{I(d)} = \mathrm{I_0 e^{-d/\lambda}}\,, \tag{2.2.3}$$

where I_0 is the initial intensity, and λ is the inelastic mean free path. After a distance λ, typically on the order of ~1 nm, one can already expect $63\% = I_0(1 - \frac{1}{e})$ fewer electrons. This sets sharp limits on where information can come from in PES. Technically, IMFP is dependent both on the propagation medium and electron kinetic energy. Practically, the behavior is universal – the specific material has only limited influence. The IMFP is mostly determined by electron energy, within a range strongly limited by binding energy and photoelectric probability[5].

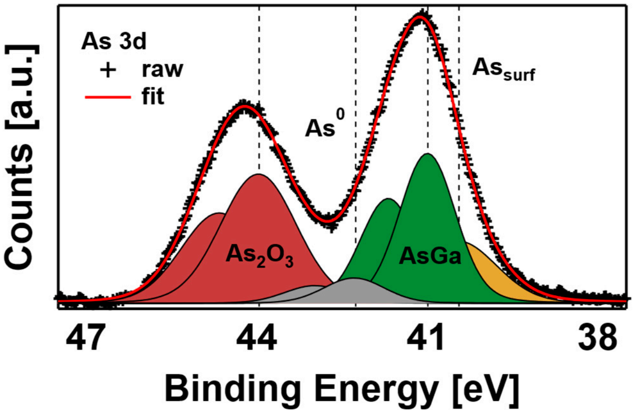

Figure 2.2.1 PES of as-grown GaAs nanowires which formed a native oxide on the surface.

2.2.1.2 HAXPES

Hard X-ray photoelectron spectroscopy (HAXPES) is an experimental attempt to increase probing depth at the expense of intensity. Fourth-generation synchrotrons like the MAX IV Laboratory in Lund, Sweden, can produce electromagnetic radiation over several orders of magnitude in energy from ultraviolet to X-ray. At the Diamond Light Source in Didcot, United Kingdom, by increasing photon energy from 50 eV to 5000 eV we were able to increase the IMFP in $Hf_2Zr_2O_4$ (HZO) from 0.5 nm to 8 nm. This was critical for work in this thesis since real devices have electrodes which control their behavior. Though unparalleled in its ability to get chemical information about buried interfaces, *operando* HAXPES is not trivial from an engineering nor measurement perspective. As mentioned in the Devices section, a top electrode several nanometers thick can be required in order to generate strain sufficient to form the ferroelectric phase of HZO. Since the signal from the interface with InAs is also diminished by several nanometers of HZO, *in situ* measurements of the semiconductor on authentic material stacks precludes the possibility of measuring through a top contact such as gold. To get around this, devices were fabricated specifically to be compatible with synchrotron beamlines. The mask pattern, dimensions and bonding had to be developed iteratively until the most effective routine was found. A schematic overview can be seen in Figure 2.2.2a where an X-ray beam at grazing incidence hits inside a gold window (~ 50 µm x 200 µm) on top of a device. This top contact has a flange out of the line of sight of the beam so that the wire can be bonded without shadowing and the device can be controlled by a source-measure unit (SMU). The bottom contact of the device is the InAs substrate which is also contacted. Comparing with the image of the sample in Figure 2.2.2b, it can be seen that tens of devices are fabricated on a single 8 mm x 10 mm wafer piece and so must be electrically isolated from one another. This is accomplished with an Al_2O_3 spacer which is sufficiently thick (80 nm) to allow wirebonding without risk of accidental shorting to the substrate. In the final iteration, ten different devices could be measured, for example at the SOLEIL synchrotron in Saint-Aubin, France, without altering the sample. This type of experimental development enabled the characterization of interfacial reactions taking place during ferroelectric switching inside real devices (see **Paper VI**).

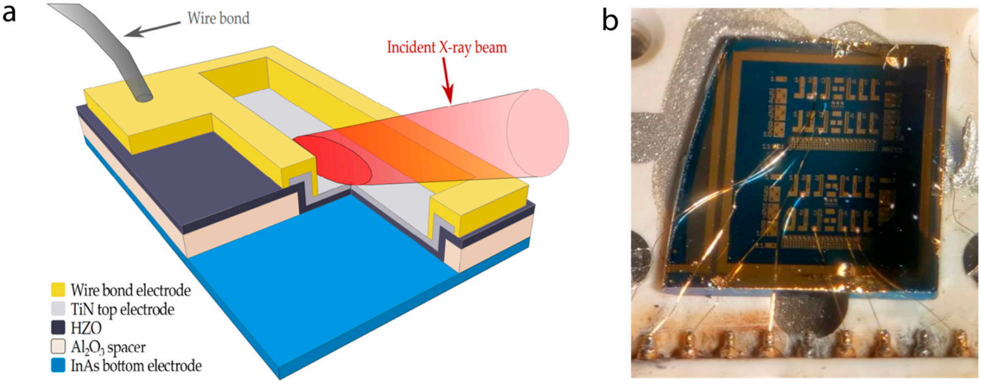

Figure 2.2.2 a) Schematic not to scale, and b) image, of operando device measurement setup.

2.2.1.3 Background, Data Treatment and Analysis

Analysis of complicated photoemission spectra which contain several overlapping peak components of varying attributes often require removal of background contributions to compare and fit data. It is sometimes observed that the background of a PE spectrum is not flat or even linear, but that there is a steplike nature to it.

This can be explained by elastic scattering from the material(s) being measured. It was explained earlier that background signal come from higher kinetic energy (lower binding energy) photoelectrons inelastically scattering on their way to the electron analyzer. If a sample contains nitrogen and arsenic, for example, excitation at 2000 eV will generate photoelectrons with 1600 eV of kinetic energy (BE_{N1s} = 400 eV). When these electrons inelastically scatter they will lose energy, and some electrons will escape the surface and reach the electron analyzer with exactly 676 eV of kinetic energy. This happens to be exactly the energy an experimenter expects arsenic photoelectrons to have (BE_{As2p} = 1324 eV). The effect is especially strong at small KEs where large numbers of secondary electrons are generated. Furthermore, this gets compounded for every atom in the sample within probing depth. Any time the retarding voltage of the analyzer is decreased (or excitation energy increased) to detect higher BE photoelectrons arriving with lower KE, all inelastically scattered primary photoelectrons and secondary photoelectrons with lower kinetic energy will also be detected. If this is significant within a single spectrum, such as the Au 4f spectrum shown in Figure 2.2.3a, then the proper method for treating and fitting the data cannot be a linear subtraction. The Shirley background[6] however is an analytical treatment which accounts for this physics. Though its calculation is rather straightforward, it deserves explanation.

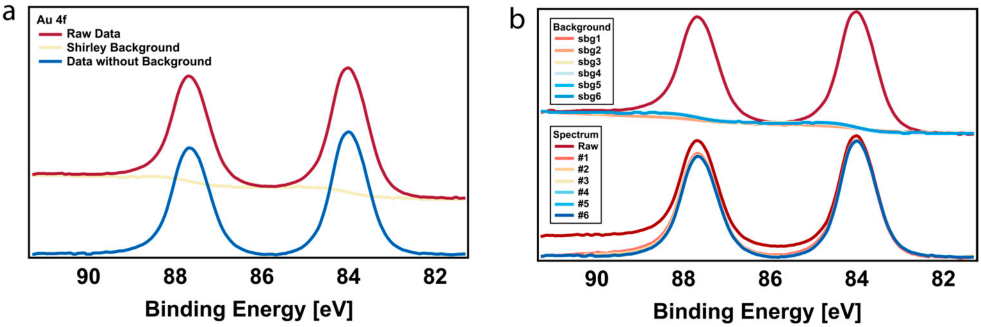

Figure 2.2.3 a) Spectra of Au 4f used for calibration with end-result Shirley background removed and b) spectra showing Shirley background iterations and convergence.

A Shirley background can be estimated by the function

$$B_S(E') = k \int_{E_i}^{E_f} I(E)\, dE, \tag{2.2.3}$$

where I is the normalized spectrum intensity at an energy E, evaluated between initial and final energies over which the background is calculated. This defines the local background in the region of the spectrum (ex. Au 4f) to be the result of that element's electrons scattering. To be appropriately scaled, the integration of the signal should be normalized by k, where $k\int_{E_i}^{E_f} I(E)\, dE = \Delta I_{i,f}$ and $\Delta I_{i,f}$ is the difference between intensities at the initial and final energies of the spectrum being subtracted. If done once, as can be seen in Fig. 2.2.3b, orange, the result is a much improved spectrum. For accuracy, the method should however be iterated since the first calculation of B_S, sbg1, is only a second estimate of the background (the first was simply I_{E_i}). B_S should then be estimated again, sbg2, based on the newest spectrum, #1, and can be subtracted from the original, Raw, to produce a more accurate spectrum, #2. In practice, as shown in Fig. 2.2.3b, only a few iterations are required before convergence.

If fitting is to be done then the peaks in PES must be assumed to have a particular lineshape. The simplest and most convenient lineshape is Gaussian, but it neglects both empirical observations and known physical processes. Intrinsic to the photoemission process, for example, there is an energy broadening which occurs due to the finite lifetime of the excited core-hole. Heisenberg uncertainty describes the fundamentally intertwined nature of physical properties such as energy and time, $\Delta E \cdot \Delta t \gtrsim \hbar$. The excited state decays exponentially, with a lifetime inversely proportional to the energies of the state. In the frequency domain, this presents as a Lorentzian distribution of energies. In atomic and certain molecular cases, the full width at half maximum of this Lorentzian broadening can be measured and used to calculate core-hole lifetime and give insight into charge-transfer processes. Since it's the intrinsic, physical photoemission processes which follow a Lorentzian distribution, subsequent processes related to measurement cause a convolution. Thermal energy distributions, phonon broadening, and experimental factors like the monochromator, electron optics, and detector response can all contribute to Gaussian broadening of the spectra. A Voigt lineshape is the convolution of a Gaussian and Lorentzian. This lineshape is not always statistically relevant to the solid state systems with significant vibrational broadening studied for this thesis. Still, it was used because of its broader applicability in the PES field and similar to the Shirely background, it being rooted in physical processes. Practically, it is advantageous to fit Voigt lineshapes with a complex error function. For this thesis, fitting was done in IGORPro 8 with the Voigt93 function. This fast and accurate[7] algorithm was developed by Josef Humlíček[8] and refined by Francis Dalaudier. Quantitative analysis becomes possible after a reasonable fitting of spectra.

Fitting a PE spectrum with a particular lineshape is not always trivial since PE spectra often have multiple peaks. The background subtracted raw data (black markers) from Figure 2.2.1 for example has two well-resolved peaks which hid two additional chemical states. This spectrum of arsenic is further complicated since it is at the binding energy of d-orbitals ($n = 3,\ l = 2$). Due to spin-orbit coupling, only s-orbitals are singlets; p, d and f electrons have two possibilities for orbital angular momentum, an energy splitting which results in the presence of PE peak doublets. Fortunately, both the energy separation and the fraction of the electrons at each spin/moment are fixed and well known – As 3d has a spin-orbit splitting of 0.7 eV and a branching ratio of 0.67, respectively. Convention adds the total angular momentum quantum number to the label of the elements shell and orbital as a subscript (i.e. As $3d_{3/2}$), where electrons with greater momentum are the more prevalent. To fit a spectrum like Fig. 2.2.1, it is greatly simplifying if the spin-orbit splitting and branching ratio are previously known, and can be fixed. A common practice is to introduce as few peaks as possible and only increase if necessary. In this case, four were needed: the GaAs bulk (green), the arsenic oxide (red), defects in between (gray) evidenced by the height of the spectrum above the background, and surface GaAs (orange). Fortunately, these have known chemical shifts, so their BE locations can be approximated while the doublets' intensities and full widths at half maximums are fit simultaneously. A good fit is not only one that matches individual data and minimizes peaks, but one that is consistent with other experimental data and known physics such as that discussed above. Typically, all electrons of an element-shell-orbital should have similar hole-lifetime, spin-orbit splitting and branching ratio.

In applied surface science, scientific and technological interest can be more focused on the interaction between finely tuned materials rather than the materials themselves. PES was frequently used for example to characterize the thin film layers of electronic devices. In **Paper II** an overlayer model was used to estimate the thickness and composition an interlayer oxide formed during the ALD of HfO_2 on InAs. When using the overlayer model it helps to make some assumptions such as flat and homogenous layer composition. To see how this can work for several thin layers stacked on top of each other, an understanding of experimental contributions to signal in PES is needed.

Emitted photoelectron intensity can be described by the equation $I = F\sigma N\lambda A$, where F is the X-ray flux, σ is the photoionization cross section, N is the number density of photoionizing atoms, λ is the IMFP, and A is the excitation area. If the experimental conditions (detector, analyzer, source, sample) aren't changed, major simplifications can be made which aid in analysis. Figure 2.2.4a is arbitrary, but models the sample in **Paper II**, where layer 1 (pink) was HfO_2, layer 2 (orange) is the interlayer InAsO, and layer 3 (blue) is the bulk InAs. Equations for intensity derived from the equation above and inelastic scattering (elastic scattering is neglected) are shown in Fig 2.2.4b. While trying to determine the thickness of the interlayer oxide, two helpful observations were made. The first is that when solving for the thickness of a buried layer, the effects of any number of overlayers can be ignored. This is because the reduction in signal intensity is identical and cancels out when intensities are divided (e^{-x} terms). The second is that when the atomic orbitals (Z, n, l) of the buried layers are the same, even if they are in different chemical states, the probability of absorbing a photon is the same. This means that $\sigma_{i+1} = \sigma_i = \sigma$. When PE intensities have been measured and λ_i and N_i are known, then d_i can be solved for explicitly. To estimate the thickness and composition of the interlayer oxide in **Paper II**, InAs spectra were fitted for two different excitation/kinetic energies. This yields two equations with two unknowns and both N_1 and d_i could be solved for.

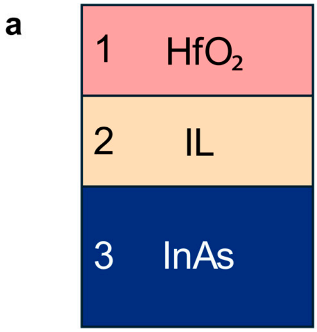

b

$$I_1 = N_1\lambda_1\sigma_1\left(1 - e^{-d_1/\lambda_1}\right)$$

$$I_2 = N_2\lambda_2\sigma_2\left(1 - e^{-d_2/\lambda_2}\right)\cdot\left(e^{-d_1/\lambda_1}\right)$$

$$I_3 = N_3\lambda_3\sigma_3\left(1 - e^{-d_3/\lambda_3}\right)\left(e^{-d_1/\lambda_1}\right)\cdot\left(e^{-d_2/\lambda_2}\right)$$

$$d_2 = \lambda_2 \ln\left(\frac{I_2N_3\lambda_3\sigma_3}{I_3N_2\lambda_2\sigma_2} + 1\right)$$

Figure 2.2.4 a, Sample schematic of overlayer model and b) equations for three layer intensities and interlayer thickness[9-12]

2.2.2 X-ray Absorption Spectroscopy

X-ray absorption spectroscopy (XAS) is a technique commonly paired with PES. For XAS, photon energy is typically scanned while drain current, fluorescence or transmission are recorded as a measure of absorption. XAS complements PES since photons can be absorbed and contribute to signal even when the excitation energy is less than the work function and no photoemission occurs. Probing unoccupied states means that absorption spectroscopy is sensitive to orbital orientation and polarization. Since X-rays penetrate matter much more easily than electrons it can also provide information at greater depth than PES. Probing deeper than PES, **Paper I** used XAS to show how increasing nitrogen gas flow during reactive sputtering resulted in the implantation of N_2 which improved device performance. Figure 2.2.5 shows an example from **Paper VI** of zirconium in a sample of TiN/HZO/InAs. Lines in absorption spectroscopy are named after the shell and orbital of the excited electron. So K-, L-, and M- edges refer to the onset of absorption which occurs for electrons with principal quantum number n = 1, 2 and 3. Within a given shell, electron energy is affected by their orbital angular momentum and spin, quantum numbers l and s, respectively. So, lettered edges are further differentiated by their total angular momentum, j, where $|l - s| \leq j \leq l + s$. The L_2 edge then signifies absorption from 2p orbitals with $j = \frac{1}{2}$. Selection rules are relevant for zirconium dioxide, so the lowest energy transition from here is to unoccupied d orbitals in the valence band. An absorption spectrum for amorphous HZO is shown as a dotted line in Figure 2.2.5. After annealing at 600 °C for 30 s however, the ~5 nm thick film was shown to have crystallized. Under similar conditions such films developed a significant orthorhombic phase which is ferroelectric. From the XAS it can be seen that the film developed long range ordering. Due to crystal field splitting, the spectrum now contains two peaks located at 2.304 keV and 2.307 keV. These represent 2p→4d transitions which have different energies due to the orientation of the d-orbitals relative to the ligands in the unit cell. That these peaks become so well resolved enables theoretical calculations and experimental fingerprinting. Based on electrical data, this is comprised of majority orthorhombic phase HZO (o-HZO). We note that it also resembles experimental and theoretical XAS[13] of tetragonal phase of ZrO_2 which is unsurprising due to their chemical and structural similarities and nearly identical lattice parameters[14]. Understanding the effects of different annealing methods used to obtain orthorhombic phase HZO was a major theme of **Papers I, III** and **V**.

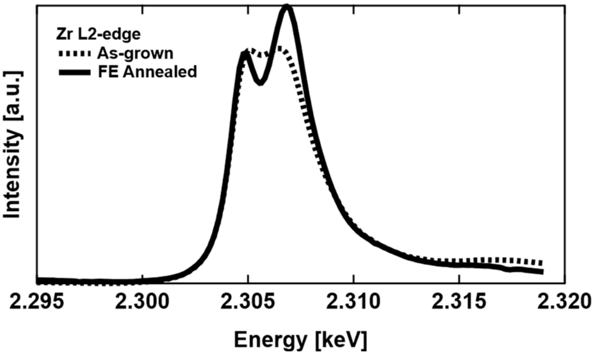

Figure 2.2.5 XAS of zirconium in TiN/HZO/InAs capacitors. Dotted line represents an unannealed, as-grown reference. Solid line represents the same sample after annealing at 600 °C for 30 s.

2.2.3 Photoluminescence Spectroscopy

Another simple yet powerful spectroscopic tool is photoluminescence (PL). This is a photon-in, photon-out technique where incoming radiation, often generated by a laser and monoenergetic, is used to excite electrons and measure reemission. Similar to absorption spectroscopy, this method provides information about unoccupied states within a material. As a relatively fast and non-destructive method, it has been a staple in bulk[15,16] and nanostructured[17,18] optoelectronic characterization for decades. In a semiconductor like GaAs, if the laser energy is sufficient then radiative recombination of excited electrons and holes provides a measure of the bandgap. In Figure 2.2.6a, the PL of GaAs nanowire arrays and a substrate reference are shown at a temperature of 100 K. Two major differences between nanowire and substrate samples are readily apparent. One is that the nanowire emission is much weaker than the substrate emission. The other is that there are two different peak positions, one at 826 nm and one at 846 nm. The first is explained by non-radiative trapping and the topic of **Paper V**. Crystals of finite size like zincblende nanowires are affected by surface phenomena like reconstruction and oxidation. At the nanoscale, a high surface-to-volume ratio compounds this effect to the point where it can literally make or break a device. The reason that as-grown nanowire samples had more than 20x less emission than the substrate was that after growth, pure GaAs oxidizes and creates defect states in the bandgap at the surface. Such states facilitate relaxation via phonons and are non-radiative recombination centers. Even on the (110) surfaces of GaAs NWs, which don't reconstruct, oxygen will replace arsenic bonds to gallium and leave behind metallic As^0 segregates. With PES it is possible to show how natively oxidized nanowires contain arsenic defects (Fig. 2.2.1, grey), and how plasma nitridation can both remove them, and prevent them in the future (**Paper V**). The difference in peak positions between substrate and nanowire emission is explained by doping. To make solar cell devices, p-doping of the substrate with zinc at n ~10^{19} cm^{-3} was used. Doping, however, changes the Fermi level of the semiconductor. Electrons excited into the conduction band are able to recombine with p-type holes just above the valence band, shrinking the apparent bandgap and the energy of the emission. The nanowires, which were not doped, emitted at the nominal bandgap of GaAs at 100 K, 1.50 eV.

Photoluminescence can be studied well beyond mere sample/dopant identification, however. Photoluminescence dynamics reveal information about electron behavior and defects which correlate with PES. To this end, time-resolved photoluminescence spectroscopy (TRPL) can be a powerful method. It is a technique where an initial pulse of energy can be used to excite the system and then photoluminescence can be tracked over time to see dynamics. This can be seen in Figure 2.2.6b where the samples were monitored over 100 ps using a streak camera. In simple, a TRPL setup involves an excitation source such as a Ti:sapphire laser, a photocathode which converts photon emission to electrons, and a streak camera, a sweeping electrode which separates the electrons in space by time, and a screen which records the signal. The ability to understand emission dynamics is powerful as it parses transitory effects which get convoluted by the steady state in PL. Just after excitation at 0 s, for example, the peak intensity of the substrate and passivated nanowires is much stronger than that of the as-grown nanowires, as seen in Figure 2.2.6a. This is due to sub-ps, fast trapping, which reduces the number of mobile charge carriers. In the 100 ps following excitation, however, there is another, slower type of non-radiative recombination which causes emission to decrease over time. Sample emission followed an exponential decay, $\mathrm{N(t)} = \mathrm{N_0 e}^{-\mathrm{t}/\tau_{trap}}$, where N is the number of electron-hole pairs, t is time, and τ_{trap} is the slow trapping rate. That $\frac{1}{\tau_{trap}}$ trapping rates decreased from 5 ps (grey) to 20 ps (blue, Fig. 2.2.6) after treatment is strong evidence that nitrogen plasma can modify and improve the surfaces of GaAs nanowire devices. Furthermore, since trapping is a reaction dependent on thermal energy, measurements can be done at two or more temperatures and activation energies calculated. In **Paper V** it was shown that passivation freezes out fast trapping, by increasing the activation energy from 30 meV to 50 meV, approximately double k_BT of room temperature.

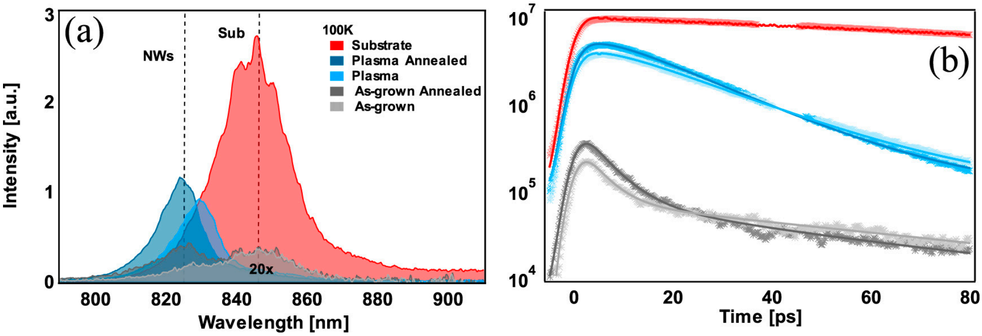

Figure 2.2.6 a) Photoluminescence spectroscopy from an array of as-grown GaAs nanowires, passivated GaAs nanowires, and a GaAs substrate at 100 K and b) time-resolved photoluminescence spectroscopy of the same arrays.

2.3 Microscopy

2.3.1 Scanning Probe Microscopy

Scanning probe microscopy techniques function based on the piezoelectric rastering of a stylus which maps the contours of a sample at a nm- to Å-scale. The field developed out of scanning tunneling microscopy (STM), which won the 1986 Nobel Prize in Physics[19]. STM is a tunneling technique and operates by measuring the quantum tunneling current generated by a potential difference between the outermost atoms of the tip and sample while their separation distance is extremely small. Though it is generally limited to both vacuum and conductive materials, the extreme sensitivity of tunneling probability to distance is what gives it unparalleled resolution in the x-y plane. That same propitious year, STM founder and German physicist Gerd Binnig published his 23,780-times citated paper introducing the atomic force microscope (AFM), a modified form of the tool functioning on the oscillations of a μm-sized cantilever which came to require neither vacuum nor electrical conduction. As Binning predicted, its sensitivity to forces as small as 10^{-18} N opened up the field of scanning probe microscopy to applications involving interatomic and even electromagnetic forces[20]. Though AFM doesn’t have Å resolution in the x-y plane, it does in z, and its flexibility and developing modes prove its perpetual utility (see Figure 2.3.1a,b).

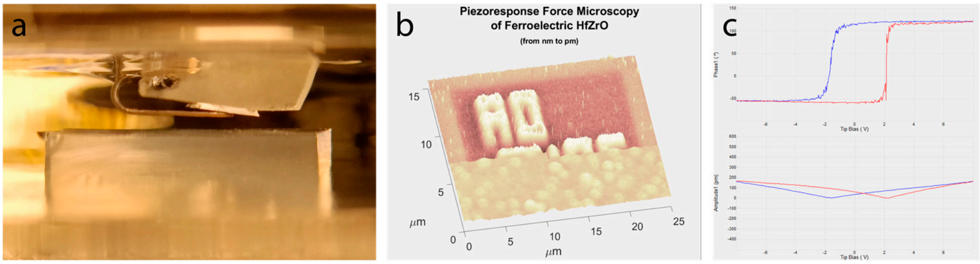

Figure 2.3.1 a) Aqueous AFM of bacteria inside a polymeric sorting device, b) PFM of ferroelectric HZO with manipulated domains spelling "Admire" in piezoresponse ~25 pm (upper half) and nanoscale topography with ~5 Å roughness (lower half). Write bias = +/- 3 V DC, read bias = +1 V AC, and c) spectroscopy on the same sample showing 180° hysteresis in phase (top) and amplitude (bottom).

2.3.1.1 *Atomic Force Microscopy*

With Å resolution in z, atomic force microscopy (AFM) offers a fast, vacuum-free characterization that makes it indispensable for nanostructure fabrication. While in-plane precision is regulated by piezoactuators, the bulk of AFM functionality comes from the interaction between a microscopic tip and a sample surface. As forces from the surface are felt by the tip, changes to the motion of the attached cantilever, such as bending, are induced. Laser light reflecting off the back of the cantilever is detected by a photodiode and deflections can be tracked and recorded by software, see Fig. 2.3.2a. Controllers can regulate this feedback and scanning set points can be maintained. After the stylus is scanned across a region of interest (nm - μm), a 3D surface image can then be made, mapping the local properties of the material. Though historically this was limited to topography, obtained via physical scraping of the AFM tip along the surface (contact mode), eventually it was found that tapping the probe (intermittent contact) was both faster and less destructive. It was further discovered that even non-contact measurements could be made of the sample surface because Van der Waals forces modify cantilever resonant frequency and oscillation amplitude. As AFM technology has developed, even more forces have been detected and newer techniques developed. Two of these, piezoresponse force microscopy (PFM) and Kelvin probe force microscopy (KPFM) require electrically conductive tips, for example platinum-iridium coated silicon. Metallic coatings allow for tip-sample biasing to probe electrical properties previously under the purview of STM and macroscopic techniques.

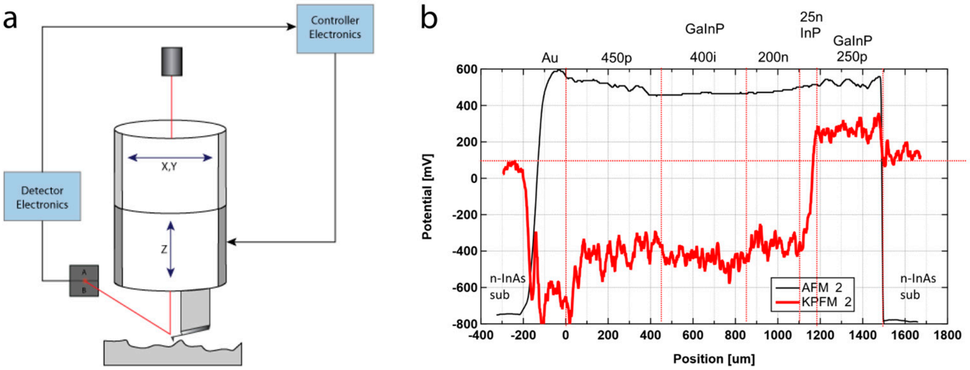

Figure 2.3.2 a) Schematic of AFM operation, borrowed from the Dimension Icon User Guide[21] and b) GaInP tandem junction solar cell NW with juxtaposed topography (black) and surface potential (red) indicating p-n junctions

2.3.1.2 Piezoresponse Force Microscopy

One advanced form of AFM is PFM. In PFM, scanning is done in contact mode while an AC bias is applied between the tip and the sample/holder which must be in electrical contact. For ferroelectric materials like o-HZO, the converse piezoelectric effect describes how an electric field across the crystal results in strain along a particular axis. An AC bias therefore will result in some deformation Δz of the sample at the frequency ω of the modulation, $\Delta z \propto \sin(\omega t + \varphi)$. With the use of a lock-in amplifier the oscillations in the cantilever at precisely this frequency can be isolated and measured, which would otherwise be negligible and lost in noise since these strain displacements are ~pm/V [22]. Using this setup, PFM is able to track both the topography and picometric oscillations of a sample surface simultaneously.

An example of this technique was applied to ultrathin HZO films annealed with ns-laser pulses and published in **Paper V**. Figure 2.3.1b shows the case of bare HZO manipulated with DC bias to write a microscopy school's name, ADMIRE, into the sample (top half). After poling with ±3 V DC, the piezoresponse of the sample could be read out with 1 V AC. Dark regions had little piezoresponse since it had domains poled opposite to the applied AC bias. Medium regions which form the image frame had an unaltered composition from growth and therefore medium piezoresponse. Bright regions had the maximum piezoresponse since domains were aligned with the applied field. In the lower half of the image, the nanoscale topography of the sample is shown by overlay. Similar to STM, PFM can also do spectroscopy. This can be done by keeping the tip in contact with the sample and sweeping a parameter like DC bias and measuring the response. Shown in Figure 2.3.1c are two common hysteresis loops indicative of ferroelectricity. For both measurements DC bias was swept between ±8 V while driving oscillations with an AC bias at 1 V. In the top figure, the phase was measured. Phase describes the oscillations of the sample relative to the AC drive bias. The zero-point is arbitrary, but perfectly in/out-of-sync is observed as a 180° shift. Hysteresis occurs because the piezoresponse of the sample depends on whether the domains are oscillating in or out of phase with the AC signal. The separation of the polarized up and down phases by 4 V corresponds to a coercive voltage of 2 V. A similar effect can be seen by measuring the amplitude of the oscillations, shown in the lower graph of Fig. 2.3.1c, where the piezoresponse goes from large down to zero and back up again, with a similar, minimal response at ± 2 V, depending on prior polarization. Though these samples were verified electrically to be ferroelectric, it should be noted that PFM is a relatively new technique and methods are still being developed[23] to isolate artifacts like charge injection from genuine ferroelectric response.

2.3.1.3 Kelvin Probe Force Microscopy

Another advanced form of AFM is KPFM. KPFM is a scanning probe technique capable of measuring the surface potential of nanostructures. For electronics strongly affected by surface properties, like nanowire-based solar cells, KPFM offers fast and flexible characterization. The technique originates from a setup developed by Lord Kelvin in the 1890's[24], where he invented the quadrant electrometer to quantify the Volta potential (contact potential difference) between two metals. In his case, it involved a capacitor of two polished discs of zinc and copper which he could connect/break electrical contact and measure the transfer of charge between the electrodes by the motion of light reflected off a mirror attached to a torsion wire.

Over a century later, modern KPFM relies on much better technology to measure essentially the same effect. When an AFM probe meets with a sample surface, the potential difference across the capacitor becomes

$$V_C = (V_{DC} - \Delta\varphi) + V_{AC}\sin(\omega_{AC}t)\ , \tag{2.3.1}$$

where V_{DC} is any applied tip/sample DC bias, $\Delta\varphi$ is the contact potential difference between the materials, and V_{AC} is any applied tip/sample AC bias with frequency ω_{AC}, at time t. The force on an AFM tip can be derived from stored potential energy when modelled as a parallel plate capacitor. When $F = -\frac{\partial U}{\partial z}$, and $U = \frac{CV^2}{2}$, where F is force, U is potential energy, C is capacitance, V is voltage and z is tip-sample separation, the resulting tip-sample force becomes

$$F_{ts} = -\frac{\partial C}{\partial z}V_C^2. \tag{2.3.2}$$

Comparing Eqs. 2.3.1 and 2.3.2 reveals that the forces acting at frequency ω_{AC} are proportional to $(V_{DC} - \Delta\varphi)$. KPFM operates by tracking the cantilever oscillation amplitude or frequency at ω_{AC} and adjusting V_{DC} until such changes are minimized. The contact potential difference is then recorded as $V_{DC} \cong \Delta\varphi$.

Paper VII demonstrated how this could be used to measure *in situ* on solar cell nanowire arrays. In that work KPFM was compared with the bulk sensitive technique electron beam induced current (EBIC) and shown to be both a complementary and non-destructive technique for mapping local changes in surface potential. This is a relevant tool for photovoltaics as it monitors dopant incorporation and the p-n junction and is compatible with other techniques. Figure 2.3.2b gives an example of *ex situ* KPFM on a more complicated, tandem junction NW where it was first removed from the array and deposited flat onto a substrate. Here the topography (black) and surface potential (red) were simultaneously mapped giving feedback on surface quality and dopant incorporation during growth. Only part of the nanowire survived the breakoff procedure used to measure these longer multiple junction nanowires, highlighting the need for developing alternative setups like cross-sectional AFM in **Paper VII**.

3 Electronics

3.1 Electronic Materials

For describing electrical behavior in solid state physics, materials are broadly classified as metals, insulators, and semiconductors. Electrons bound to single atoms are confined to particular energies and regions called orbitals. In solids like crystals, the atoms are numerous and densely packed, leading to orbital overlap and the formation of broad, continuous energy bands. Depending on how these energy levels and bands compare to each other, conduction can occur. In Figure 3.1.1 we see band diagrams for metals, semiconductors and insulators where the energy of the electron state is on the y-axis and the density of the states is on the x-axis. The Fermi level is the energy at which there is a 50% probability for occupation by an electron[25]. This implies that at 0 K, i.e. without any thermal energy, all states up to the Fermi level are filled and all states above the Fermi level are empty. For metals, this energy is in the middle of a band, implying that continuous electron states exist both above and below. For a perfect semiconductor, the Fermi level lies within a gap in the bands, though it can be modified by defects or doping which creates states nearer to the filled valence band or unfilled conduction band. Insulators have such a large bandgap that essentially no electrons can occupy the delocalized states of the conduction band and are non-conductive. Different constellations of these types of materials can be used to form capacitors, resistors and transistors, allowing for precise control over the flow of charge and leading to much of the technology we rely on today. A few examples which formed the backbone of the research included in this thesis: ReRAM, FTJ, FET, p-n junction, will be explained in greater detail below.

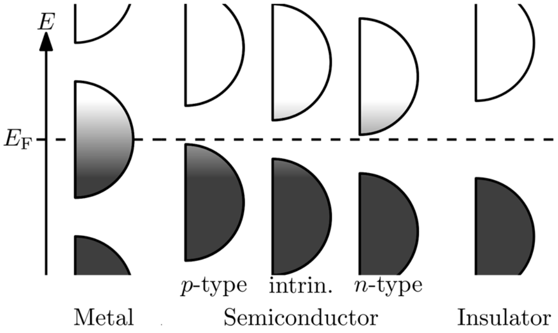

Figure 3.1.1 Electron band diagram for different materials. Image adapted from Nantite[26]and Kittel[27].

3.1.1 Crystals

A crystal is a highly ordered macroscopic solid composed of microscopic repeating units. Particular atomic arrangements are called phases and are classified by their symmetry, or space group. The insulators HfO_2, ZrO_2 and related compounds of different Hf/Zr ratios like $Hf_2Zr_2O_4$ (HZO) can be found amorphous, lacking crystallinity, polycrystalline, containing multiple crystal grains or phases simultaneously, or single crystalline, composed of just a single crystal phase. Though many different crystal phases exist for HZO, only some of them are thermodynamically stable in ambient. Of these, many fewer are likely to form or persist during standard processes in a lab or production facility[28]. Though amorphous HZO is quite easy to form through chemical vapor deposition (CVD) techniques, crystalline phases, and in particular the non-centrosymmetric, orthorhombic phase which is ferroelectric, requires high temperature and/or pressure to form[29]. It is the $Pca2_1$ space group (orthorhombic III) which is generally assumed to be responsible for ferroelectricity in HZO[14]. A ball and stick model for this crystal structure is shown in Figure 3.1.2a. It is a cubic-like lattice with orthogonal but stretched lattice parameters (i.e. orthorhombic) which in HZO are approximately a = 5.05 Å, b = 5.27 Å and c = 5.08 Å[30].

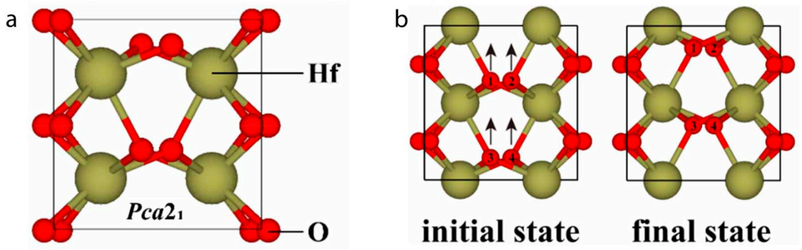

Figure 3.1.2 a) Ball and stick model of the $Pca2_1$ space group for HfO_2, the orthorhombic, ferroelectric phase and b) oxygen relocation as the source of polarization switching. Images generated by VESTA and adapted from Ge-Qi Mao et al.[31]

3.1.2 Insulators

3.1.2.1 Hafnia

Hafnium oxide (HfO_2) plays a crucial role in modern electronics, particularly in memory and transistor technologies, due to its exceptional electrical properties. Its high dielectric constant (high-κ) makes it an ideal insulator for transistor gate dielectrics. Hafnia's robustness, thermal stability, and compatibility with ubiquitous silicon processes make it indispensable in semiconductor manufacturing. Beyond traditional applications, its ability to form conductive filaments and exhibit ferroelectric properties paves the way for innovative components like memristors.

3.1.2.2 Ferroelectricity

Materials which demonstrate both a spontaneous and reversible electric polarization are said to be ferroelectric. This is a subproperty of pyroelectricity which doesn't require reversibility under an applied electric field[32,33]. These are both, necessarily, piezoelectric which is why PFM is such an effective technique for characterizing them. That charge separation can be maintained in the absence of an electric field is critical to the functioning of ferroelectric memory devices. One polarization state can act as a zero while the flipped polarization state represents a one. In FTJ capacitor, this state can be measured by the amount of current tunneling through the insulating oxide. In FeFET and FeRAM the polarization state modulates the channel conductivity and charge on the memory capacitor, respectively. These are schematically illustrated in Figure 3.2.1.

A common method for switching ferroelectric devices is the (positive-up negative-down) PUND method. An example from TiN/HZO/InAs capacitors is shown in Figure 3.1.3. During the synchrotron experiments conducted for **Paper VI**, FE devices were controlled by a portable Keithley B2900 source-measure unit. To do a PUND measurement the ferroelectric layer starts by being initialized to a particular state, for example polarized down with a negative bias placed on the top electrode. Next, a *positive* voltage pulse is applied which will flip the FE polarization state to the upward orientation. During this polarization switching, a FE current is generated due to the relocation of charges within the film. Crystallographically, this results from the relocation of oxygen atoms within the lattice, as in Figure 3.1.2b. A subsequent, identical, *up* pulse then follows which demonstrates the retention of the polarization state via no current response (except minimal leakage and/or dielectric currents). Next, the cycle is completed with two inverted voltage pulses, *negative* and *down*. When the polarization is reversed back to down by a *negative* bias, a FE current is again recorded. Such current is not seen on the fifth and final, *down* pulse for the same reason as before. PUND measurements were critical for this research not just because it can set the polarization states for X-ray measurements, which DC bias can do, but also because it verifies and measures the FE response, including state retention. This is because FE current shows a unique, non-ohmic response, yet once the state is set subsequent pulsing induces no FE current. Such a method is therefore well-suited to provide the fast control, feedback and characterization required for *operando* synchrotron studies.

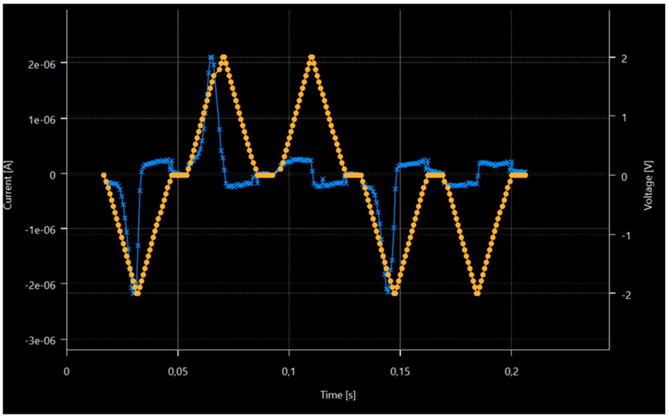

Figure 3.1.3 PUND measurement of ferroelectric TiN/HZO/InAs capacitor during synchrotron measurements which recorded applied bias (2 V > V > -2 V, orange dots), and ferroelectric current response (2 µA < I < -2 µA, blue line)

3.1.3 Semiconductors

3.1.3.1 III-Vs

III-V materials, compounds formed by elements from groups III and V of the periodic table, are fundamental in semiconductor technology due to their unique electronic and optical properties. Known for their high charge carrier mobility, these materials enable faster electron transport, making them ideal for high-frequency and high-speed applications like transistors and integrated circuits. Their direct bandgap facilitates efficient light emission and absorption, essential for optoelectronic devices such as LEDs and solar cells. GaAs and InP, for example, have a direct bandgap around 1.34 eV, the most efficient for solar light absorption[34,35]. Whether it is for radiation-hard, ultra-high efficiency tandem junction solar cells used in space[36,37], faster 5G telecommunications, or memristors for in-memory computation, the ability to engineer their bandgaps and Fermi level through alloying and doping enhances III-V versatility. This allows optimization in a broad range of next generation technologies.

3.1.3.2 Semiconductor surfaces

Semiconductor surfaces possess unique properties due to their atomic structure and electronic characteristics. Key aspects include surface states, which are electronic states within the bandgap that can trap charge carriers and affect electrical properties, leading to phenomena such as Fermi level pinning that influences energy band alignment and junction behavior. Another critical feature is dangling bonds, which result from the termination of the crystal lattice at the surface, creating highly reactive sites that can significantly alter the surface chemistry and electronic behavior. These dangling bonds can lead to increased surface recombination, impacting, for example, photovoltaic efficiency. Additionally, semiconductor surfaces are prone to oxidation. Silicon surfaces react to form silicon dioxide, a passivation layer serendipitously useful for creating electrical isolation and protection against contamination and electrical interference. In contrast, III-V semiconductors are known for their unfavorable native oxides which may contain defects, a major motivation for the work done in **Papers II, III, IV and VI**. The unique properties of semiconductor surfaces are fundamental to the design and optimization of various electronic and optoelectronic devices, strongly influencing their performance, reliability, and functionality. Whereas **Papers III, IV and VI** were concerned with minimization of interfacial reactions of InAs and GaAs with oxygen, **Paper II** highlighted an exception to the rule. Deliberate oxidation of the HZO/InAs interface was found to reduce breakdown and increase ReRAM stability. Ultimately, understanding and controlling application-specific surface characteristics is essential for advancing semiconductor technology and developing new applications.

3.1.3.3 Passivation

Unlike **Papers III and V** where the goal was to find ways to avoid interfacial reactions by reducing exposure to thermal energy, **Paper IV** was motivated by the desire to remove existing electrical defects and prevent their reformation – passivation. Passivation can be seen both chemically and electronically. Chemical passivation often takes the form of a coating, and acts like a physical barrier which prevents mixing and reactions, maintaining the purity of the passivated material. Electronic passivation describes the elimination of unwanted electronic states and isolation from other device components. The surfaces of GaAs NWs from **Paper IV** were shown to have severely oxidized in ambient, which introduced electronic defects in the bandgap. Optoelectronically, this results in midgap states which trap the free electrons created by light absorption, and is measured by reduced photoluminescence. As described in section 3.1.4.2 on plasma processing, hydrogen radicals were used to remove oxygen and segregates of As and nitrogen radicals were used to replace As and make GaN. GaN achieves electronic passivation for GaAs because of its much wider, straddling bandgap alignment. PES was used to show that this nitridation produced a surface GaN capable of chemically passivating NWs on the timescale of years.

3.1.4 Growth and Processing

In order to characterize advanced materials, equally sophisticated tools must first be employed to actually produce them. A brief overview of some of the more fundamental techniques behind sample fabrication will be discussed below.

3.1.4.1 Metalorganic vapor-phase epitaxy

Metalorganic vapor-phase epitaxy (MOVPE) is a chemical vapor deposition technique where crystalline materials are formed with the use of reactant precursors in the gas phase. Etymologically, epitaxy literally means ‘ordered on top’ and gets its name because crystal growth follows lattice-matched from a substrate template. This gives it extreme control over growth phase and orientation. Unlike techniques such as molecular beam epitaxy, MOVPE can quickly fabricate nanostructures with modest vacuum requirements, making it indispensable for the production of semiconductor devices. For the solar cell nanowire arrays studied for **Paper IV** (**Paper VII**), trimethylgallium (trimethylindium) and arsine (phosphine) were used as precursors to grow GaAs (InP) freestanding light absorbers. MOVPE growth of III-V nanowires often uses the vapor-liquid-solid (VLS) method[38-40] and began with an array of Au particles deposited using nanoimprint lithography and evaporation. The vapor-liquid-solid growth model is used to explain how reactor gases mix with the liquid gold on the substrate surface and then thermodynamically favor reaction at the low surface energy interface between the wafer (and eventually nanowire) and the gold. As the compound semiconductor begins to form within the lithographic pattern, the direction of crystal growth as well as phase and dimensions is fixed for subsequent freestanding growth of up to several micrometers. Temperature, gas composition and pressure, cleanliness and time are critical parameters for high quality structures. Though III-V semiconductor growth was not the main subject of the work in this thesis, the cleaning, modification and characterization of these surfaces was the topic of interest in **Paper IV**.

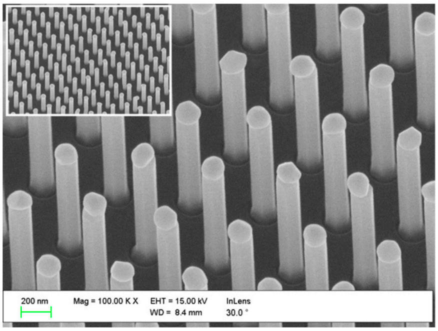

Figure 3.1.4 SEM micrograph of GaAs nanowire array used for photovoltaics. Nanowires are terminated with Au particles which are critical to growth.

3.1.4.2 Plasma

For the cleaning and surface conversion of nanowire arrays a Fiji F200 remote inductively coupled plasma (ICP) source made by Cambridge NanoTech was used. Plasma-enhanced CVD has become a staple in modern laboratories and fabs because of its balance of relatively low processing temperatures with high film quality and deposition speed. As explained in **Paper IV**, the ICP setup employed for photovoltaic nanowires actually avoided the direct use of plasma, instead opting for a gentler, remote setup with a physical separation between the plasma generation and the sample. The result of such a design is that only radicals and neutral gas species, but not more aggressive and potentially defect-causing ions come into contact with the sample. For simplicity however, the term plasma will be used regardless to describe the process. For the nitridation of GaAs nanowires it was necessary to first remove the native oxide produced by exposure to ambient. This was done with a brief H_2 plasma which is highly reactive to Ga- and As- oxides and their byproducts easily desorb at 250 °C. At a slightly higher temperature of 350 °C a mixed plasma of 97% N_2 - 3% H_2 was used to convert the gallium rich surface to GaN. The inclusion of 3% H_2 was found to be critical as it prevents oxide formation and arsenic from accumulating during nitridation. Reduction of As^0 was correlated with improved metrics like increased luminescence and fewer trap defects in GaAs solar cell nanowire arrays, similar to much of the research on ferroelectric HZO/InAs interfaces presented in this thesis. Optimizing III/As interfaces was shown to be attainable through other methods as well. Especially for HZO/InAs configurations controlling exposure to thermal energy was found to be essential.

3.1.4.3 Atomic Layer Deposition

Plasma can also be used to enhance atomic layer deposition (ALD). Unlike in CVD, ALD separates reactants during the growth process which allows for monolayer, conformal deposition. This is because ALD relies on self-limiting reaction steps typically beginning with a flux of reductant. In the case of hafnium oxide, for example, tetrakis(dimethylamido)hafnium (TDMAHf) has been used. These metal-organic precursor gases are essentially metal atoms surrounded by methyl ligands which react with and become replaced by surface oxygen. Once the surface is saturated with ligand terminated hafnium, additional deposition becomes thermodynamically unfavorable and the reaction chamber can be purged with an inert gas and a new precursor gas introduced. To complete the layer, water can be used as an oxidant. During this step the final ligands of the metal are removed and an OH-terminated oxide remains. Purging completes the second half-cycle and a monolayer is formed. Because ALD can precisely control the type and number of surface reactions, it has become a staple of the semiconductor industry. The isotropic nature of gas flows and its self-limiting nature also makes ALD perfect for thin films on three dimensional structures.

For the work presented in this thesis, ALD was the method of choice for depositing thin, conformal, stoichiometric layers of HfO_2, ZrO_2, and HZO. **Paper II**, for example, reports the surprising observation that, when fabricating nearly identical ReRAM and MOSFET structures on the same InAs nanowire, adjusting the hafnium oxide ALD completely changed device performance. Whereas it has typically been found that clean, native oxide- and defect- free interfaces between III/V semiconductors and high-κ materials are essential for high performance transistors[41,42], these produced poorly performing ReRAM. Instead, an extended oxygen plasma during the second half cycle was explored. The use of a plasma oxidant as an alternative to water is called plasma-enhanced atomic layer deposition. On planar samples fabricated to mimic the smaller, three-dimensional NW devices, it was found that increasing the O_2 plasma time from 10 s to 80 s during the first ten ALD cycles dramatically affected the devices. First, compared to the self-cleaning ALD used on the MOSFET, the HfO2/InAs of the ReRAM had a nanometers thick InAs interlayer oxide. It was shown that the thickness of this oxide was controllable by adjusting the length of the exposure. Furthermore, we report that it is precisely this interlayer oxide that, when sufficiently thick (about 3 nm), actually allows for a high-performance ReRAM. Increasing O_2 plasma exposure resulted in an improved memory window.

3.1.4.4 Sputtering

Sputter deposition is a form of physical vapor deposition (PVD) where ions of an inert gas ballistically collide with a target material causing the ejection of atoms and anisotropic deposition onto a sample substrate. What sputtering lacks in atomic layer control compared to CVD and ALD it makes up for with simplicity and speed. It requires no chemical reactions, relying only on pure targets and noble gases like argon or neon. Because it is a mere physical transfer of atoms, it operates at much lower temperatures and can make thicker films in less time. After amorphous HZO is deposited through ALD, for example, many nanometers of a metal electrode are needed to make electrical contact with the oxide and to strain-engineer the transformation to the ferroelectric phase. Sputtered electrodes are the simplest and most efficient.

In **Paper I** it was shown how the parameters of TiN sputter deposition could be used to influence film growth, defect concentration and remanent polarization after annealing. In this work, RF magnetron sputtering with the inclusion of reactive nitrogen was characterized. With a TiN target, it was found that argon pressure could be increased to promote growth of (111) terminated cubic TiN, introducing the tensile stress needed to produce o-HZO. The introduction of N_2 during deposition however was found to promote ferroelectric crystallization despite increasing reactive nitrogen which is associated with compressive (002) growth. With the help of XAS and XPS it could be suggested that N_2 flow served two purposes. First, it physiosorbed and incorporated into the sample matrix providing the appropriate strain for crystallization[43]. Second, it provided sufficient nitrogen for stoichiometric film growth. Devices with increased nitrogen concentration were found to have significantly fewer defects, decreasing oxygen scavenging from the HZO, and resulting in an order of magnitude increase in device endurance.

3.1.4.5 Annealing

As mentioned earlier, the successful conversion of amorphous or non-FE HfO_2 to the orthorhombic phase requires a combination of temperature and stress, as the phase does not spontaneously form in ambient. To achieve this, especially for thin films, usually some combination of doping, straining with electrodes, and annealing are used. **Paper I** is an example where rapid thermal processing (RTP) at 440 °C was used in conjunction with a capping top electrode to provide the necessary stress for ferroelectric phase conversion in HZO. Doping and annealing alone are insufficient to produce high quality devices, however. In that study it was found that by tuning gas composition and pressure during electrode sputtering the strain in the layers could be controlled to promote an orthorhombic transformation of HZO. Though heat treatments are ubiquitous in the preparation of electronic materials and devices, they do not come for free. III/V semiconductors dissociate and desorb much sooner than silicon. Even at 440 °C As begins to desorb from surfaces[44]. In **Paper III** a faster, flash lamp annealing (FLA) technique was compared with traditional RTP to understand the influence of time on the FE-semiconductor interface and sample temperature. Unlike with RTP, which provides a uniform distribution of heat to the sample on the timescale of seconds to minutes, FLA is able to crystallize HZO with a 3 ms pulse of intense white light. This results in a temperature profile within the sample stack heavily skewed toward sample surface. PES measurements showed that the reduced time spent at elevated temperatures resulted in a significant reduction in defect density and therefore better endurance, despite maintaining strong ferroelectricity. Multiple FLA pulsing was found to enhance the somewhat weaker remanent polarization. A much rarer nanosecond laser annealing (NLA) technique was also demonstrated, in **Paper V**.

3.2 Devices

Much of the research presented in this thesis was aimed at pushing existing technologies into the future via reducing the size, increasing the efficiency, and/or adding functionality to existing electronic devices. Four such devices which underpin these publications are FTJ, ReRAM, FET and photovoltaic cell and will be discussed as an introduction to these texts.

3.2.1 FTJ

One novel memory application for ferroelectrics is called a tunnel junction (FTJ) and can be seen in Figure 3.2.1c. This is a thin film capacitor structure with a ferroelectric insulator between two conductive electrodes. Due to ferroelectric polarization, the internal electric field induces a charge buildup at the interfaces. This redistribution of charge modifies the electric potential across the gap, resulting in a polarization-dependent tunneling electroresistance. That the tunneling barrier across the FTJ can be switched for OFF/ON resistance ratios greater than 10^4 means that a large memory window can be achieved on very thin films[45]. Since the state is read out at $V_{read} \ll V_{switch}$, it is non-volatile. The power saved combined with increased endurance give it potential for the next generation of flash memory[46]. Furthermore, its fast switching speeds mean it also has potential for RAM.

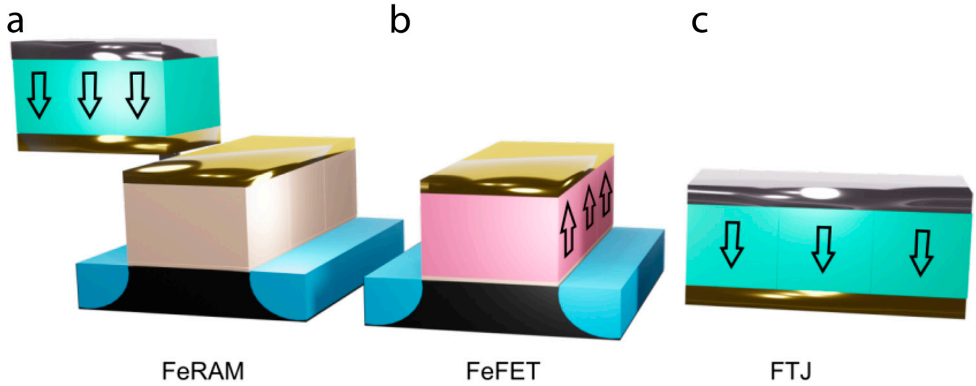

Figure 3.2.1 Overview figure of the three promising ferroelectric device concepts. (a) FeRAM consisting of 1T-1C where the storage capacitor is a nonvolatile ferroelectric. (b) FeFET, where the ferroelectric material is integrated as the gate oxide and the polarization direction can promote either accumulation or depletion in the semiconducting channel, changing the threshold voltage Vt . (c) FTJ, where the ferroelectric is sandwiched between two metal electrodes, and the transmission probability of charge carriers is dependent on the polarization direction of the ferroelectric. Image borrowed from R. Athle[47]

3.2.2 MOSFET

The metal-oxide-semiconductor field-effect transistor (MOSFET) is perhaps the fundamental building block of the modern computer, and its various forms allow it to fulfill a wide range of roles from control, to processing, and memory. The basic structure of the MOSFET is a three-terminal device where conduction between the source and drain can be modulated by a gate. The gate often has a metallic electrode contacting an insulator made of an oxide which contacts a semiconductor, the medium between the source and drain, hence the name. Acting like a switch, the application of bias to the transitor's gate electrode creates an electric field across the oxide and changes the conductivity in the channel. The resistive state signifies 'off' or a 0, and the conductive state represents 'on' or a 1, giving it the basic functionality for both memory and routing. In the case of flash memory, the slower, longer lasting memory used by USB and solid-state drives is built up of floating-gate MOSFETs, where an additional conductor sits isolated between the channel and control gate. Charge in this floating gate becomes the memory unit. Reading the current from the transistor checks the memory, since, when (un)charged, the floating gate does (not) screen the influence of the gate on the channel. Though a very effective tool, modern flash memory isn't very fast or energy efficient and has limited endurance. This is where ferroelectrics offer significant advantages.

3.2.2.1 FeFET

A ferroelectric metal-oxide field-effect transistor (FeFET) obviates the need for a floating gate by replacing all of the insulating layers between the gate and the channel with a single ferroelectric oxide (Fig. 3.2.1b). The FE layer functions both as the gate oxide which modulates the channel conductivity, and the memory unit, because it is the retained polarization state which influences screening. To set the memory state, the coercive voltage V_{coer} can be applied to the gate, changing the polarization within the FE oxide. Reading the memory with $V_{read} \ll V_{coer}$ results in either a low or high source-drain current where $I_{off} \ll I_{on}$. The memory window of a FeFET is the voltage separation required to read out two or more distinct states. That partial polarization switching can be utilized to create additional non-binary states means potential neuromorphic applications also become relevant.

3.2.3 RAM

Random-access memory (RAM) is the main memory of a computer and is known for its fast read and write speeds. The price of this speed, besides the direct financial cost of production, is volatility. Unlike larger data storage on drives, computer memory typically requires the power to always be on to maintain the voltage state of a transistor or refresh the charge state on a capacitor. The modern DRAM cell is made of a MOSFET and a charge storing capacitor, where the (un)charged state represents an 'on'('off') or a 1(0). Significant additional circuitry and energy is required to constantly read and rewrite the charge state of these leaky devices. Though this weakness of RAM puts a burden both on the environment and the consumer, it also opens up opportunity for new technologies that are non-volatile and more energy efficient.

3.2.3.1 ReRAM

Resistive random-access memory (ReRAM) is one of the most promising technological alternatives to modern 1-transistor 1-capacitor memory. Instead of storing charge on a capacitor, or even FE polarization in the case of FeRAM, ReRAM employs a type of variable resistor which can represent a memory state depending on how conductive it is. As shown in Figure 3.2.2c, high and low resistive states, for example, can be programmed into the oxide by applying voltages which either form or break a conductive filament through the insulator. These filaments are typically composed of charged, mobile oxygen vacancies. A low-resistance state for example can be set by applying a large bias across the device which reduces the oxide at certain locations, a reaction which locally shorts the device creating a much more conductive path for charge to flow. Reverse bias, on the other hand, can reoxidize the layer, break the conductive filament, and reset the device. The current output from a ReRAM device indicates the memory state where $V_{read} \ll V_{set}$. Such devices were the subject of **Paper II**, shown in Figure 3.2.2a,b. A single InAs nanowire with hafnium oxide was demonstrated to support both the formation of a transistor and a resistive memory component. A key finding was that ALD should be tuned to meet the interfacial demands of these unique components. Though MOSFET performance has been shown to deteriorate with any oxide or defects at the semiconductor interface, the ReRAM component was very different. In fact, deliberate oxidation during ALD with oxygen plasma was shown to increase the stability of the resistive switching[48]. The In- and As- oxide rich interlayer acts as an oxygen reservoir enabling redox during filament formation/removal. Furthermore, as a voltage divider, the interlayer helps with current compliance increasing endurance by preventing breakdown of the device.

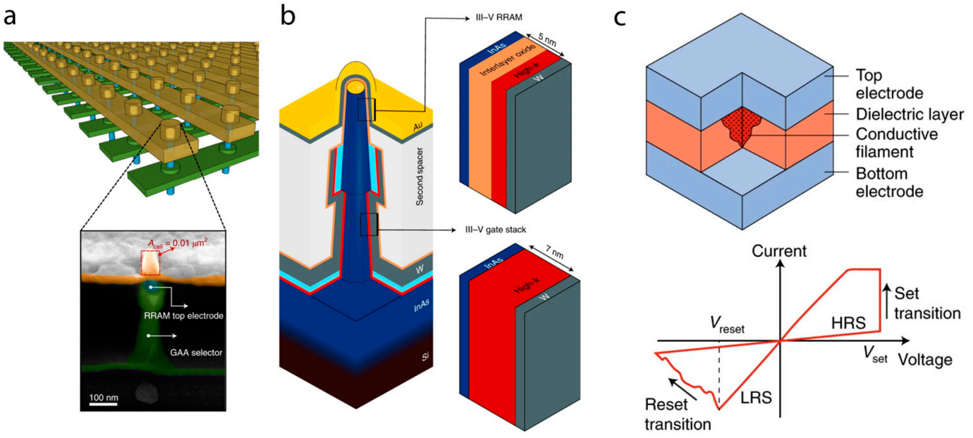

Figure 3.2.2 a) Crossbar array of ReRAM memory, inset: SE micrograph. b) schematic of a single vertical nanowire ReRAM device with 1-transistor and 1 resistor. c) schematic of filamentary formation during the set procedure (top) model I-V behavior of ReRAM in low and high resistive states (bottom) Adapted from R. Carboni et al.[49]

3.2.4 Solar Cell

A solar cell is a device which converts energy from photons (i.e. sunlight) into electricity via the photovoltaic effect. The most common photovoltaic devices providing solar energy to today's society are based on a specific arrangement of semiconductor materials called a p-n junction (see Fig. 3.2.3b). P-n junctions are where semiconductor materials doped with acceptors/donors meet. As shown in Fig. 3.1.1 these regions have a Fermi level close to the valence/conduction band. The proximity of mobile electrons to holes allows for the creation of a space charge region in which, due to diffusion, the n-type electron donors leave behind a positive charge and the p-type hole acceptors leave a net negative charge. Just like in PL, incoming solar radiation has enough energy to excite bound electrons in the valence band across the bandgap into the conduction band. As highlighted in Figure 3.2.3a, the built-in electric field from the p-n junction drives the collection of these photoexcited charges created by sunlight and provides the current for our electricity. Finding ways to increase the efficiency of this process is one way to make solar energy cheaper and more useful to society. One of the most efficient materials for the conversion of sunlight to current is the III-V semiconductor GaAs, because its bandgap (1.42 eV) absorbs much of the solar spectrum without wasting too much of the energy to heat. This is complemented well by miniaturization in the form of nanowire arrays and aerosols which decrease the amount of raw material required and allow for flexible integration schemes.

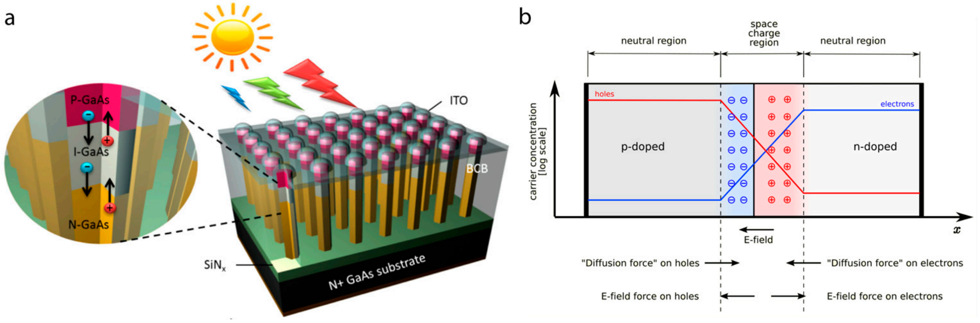

Figure 3.2.3 a) Illustration of GaAs NW array solar cell with p-n junctions and b) model of p-n junction with space charge region and electric field. Images adapted from TheNoise[50] *and M. Yao et al.* [51]

To really maximize the benefits of high-efficiency semiconductors at the nanoscale, however, surface effects must be understood and accounted for. **Paper I** is concerned with the treatment of GaAs nanowire surfaces for improved efficiency. It was found that nitrogen plasma could be used to replace As with N on the outside of NWs. Through the use of PES and TRPL, this was found to remove As defects which trap electrons and interfere with photovoltaic conversion. Critically, GaN has a much larger bandgap than GaAs so charges are electrically confined to the NW bulk and don't interact with surface states. Further, this surface passivation was shown to be stable for more than a year. **Paper VII** used KPFM on similar InP arrays to investigate electrostatics across the p-n junction on photovoltaic NW surfaces. In that work AFM was conducted directly on the nanowire array. As a scanning probe technique, this method demonstrated the ability to complement bulk sensitive techniques like EBIC, in ambient and without removal from the growth substrate.

4 Concluding remarks

The breadth of research presented in this thesis covers advancements into the fabrication and operation of electronic nanomaterials and devices. Characterization of these metals, oxides and semiconductors focused on their interfaces and developing techniques to improve their stability and performance. This diverse work spans key areas of nanoelectronics from photovoltaics to circuit elements, and seeks to improve the readiness of promising technologies. To do this, a combined suite of scanning probe and X-ray techniques was used to provide a broad understanding of structural and electronic properties. Scanning probe techniques such as Kelvin probe force microscopy and piezoresponse force microscopy were able to provide local, surface characterization down to the nanoscale. Piezoresponse force microscopy helped corroborate the formation of ferroelectric thin films by reversibly switching domains and measuring electrical hysteresis. Kelvin probe force microscopy was found to complement electron beam induced current in the investigation of photovoltaic p-n junctions, and was used to highlight a unique method for nondestructively measuring directly on nanowire arrays. Visible light was used in photoluminescence spectroscopy to gain access to the bulk of photovoltaic nanowires, where temperature- and time-dependent measurements showed how nitrogen plasma treatment increased GaAs solar cell efficiency. Complementary PES provided surface sensitive information, demonstrating surface conversion to GaN and long-term passivation. With the help of synchrotrons such as MAX IV, high flux X-ray radiation enabled probing below the surface of thin films for novel circuit components. X-ray absorption spectroscopy helped to explain reactive sputtering of TiN, connecting electrode texturing with the formation of HZO's ferroelectric phase and increased endurance in devices. Photoemission was repeatedly used to understand the impact of device fabrication on their thin film components. For resistive random-access memory devices it revealed the importance of ignoring conventional wisdom and forming interlayer oxides which protect key functionality. In ferroelectric devices it proved the opposite, highlighting the necessity for short timescale thermal processes by consistently linking the breakdown of devices to film decomposition. Finally, *operando* hard X-ray photoelectron spectroscopy was employed to follow ferroelectric switching in real time. Synchrotron compatible devices were developed, and characterization of buried interfaces revealed a polarization dependent, reversible redox between HZO and InAs which, if left unchecked, ultimately leads to breakdown.

Future work in these areas will necessarily continue to concentrate on semiconductors applications and interfaces. For solar cells, Kelvin probe force microscopy on multi-junction NWs is interesting, as they offer increased efficiency at the cost of complexity. Rapid, in situ feedback to growers offers a characterization that doesn't sacrifice precious samples and can be incorporated into complete device fabrication routines. As tandem junction NWs have challenges both with dopant control and surface passivation, photoluminescence spectroscopy and atomic force microscopy remain promising techniques to increase technical expertise and push exploratory research toward operational technology. Resistive random-access memory work may continue along the lines of *operando* X-ray studies. It would be interesting to know how big a role remanent polarization, doping, and applied fields play in the switching chemistry of HZO/InAs reactions. Furthermore, as arsenic compounds have been demonstrated to decompose and create defects, interchanging InAs with other semiconductor compounds like GaAs or GaN may offer benefits to key performance metrics like endurance, which still need improvement. Additionally, preliminary chemical and electrical data suggest that incorporating an interlayer, such as Al_2O_3 between HZO/InAs, can act as a diffusion barrier and increase device stability. Hard X-ray photoelectron spectroscopy studies in particular would be well suited to characterize these buried interfaces in realistic device arrangements. To that end, replacing unstable top electrodes like TiN and W with thin, low atomic number, nonreactive conductors, like graphene, would facilitate characterization. Finally, though much work and success has been achieved in developing alternative annealing processes to effect the ferroelectric phase transformation, non-annealing methods should be considered carefully as they offer increased compatibility with both III-V materials and back end of line industrial processing. Generally, this work has further confirmed that, independent of the specific material and device application, it is crucial to have a large characterization toolbox at hand, especially one that includes surface-sensitive techniques tailored for *operando* measurements at the micro- and nanoscale.

References

1 Index, C. B. E. C. *Bitcoin Network Power Demand*, <https://ccaf.io/cbnsi/cbeci> (2024).

2 SCB. *Tillförsel och användning av el 2001–2022 (GWh)*, <https://www.scb.se/hitta-statistik/statistik-efter-amne/energi/tillforsel-och-anvandning-av-energi/arlig-energistatistik-el-gas-och-fjarrvarme/pong/tabell-och-diagram/tillforsel-och-anvandning-av-el-20012022-gwh/> (2023).

3 OpenAI. *ChatGPT, Large Language Model*, <https://chat.openai.com/> (2024).

4 AB, N. P. O. Wilhelm Conrad Röntgen – Facts. (2024).

5 Seah, M. P. & Dench, W. A. Quantitative electron spectroscopy of surfaces: A standard data base for electron inelastic mean free paths in solids. *Surface and Interface Analysis* **1**, 2-11, doi:https://doi.org/10.1002/sia.740010103 (1979).

6 Shirley, D. A. High-Resolution X-Ray Photoemission Spectrum of the Valence Bands of Gold. *Physical Review B* **5**, 4709-4714, doi:10.1103/PhysRevB.5.4709 (1972).

7 Schreier, F. The Voigt and complex error function: A comparison of computational methods. *Journal of Quantitative Spectroscopy and Radiative Transfer* **48**, 743-762, doi:https://doi.org/10.1016/0022-4073(92)90139-U (1992).

8 Humlíček, J. Optimized computation of the voigt and complex probability functions. *Journal of Quantitative Spectroscopy and Radiative Transfer* **27**, 437-444, doi:https://doi.org/10.1016/0022-4073(82)90078-4 (1982).

9 D'Acunto, G. *et al.* Atomic Layer Deposition of Hafnium Oxide on InAs: Insight from Time-Resolved in Situ Studies. *ACS Applied Electronic Materials* **2**, 3915-3922, doi:10.1021/acsaelm.0c00775 (2020).

10 Mohai, M. & Bertóti, I. Calculation of overlayer thickness on curved surfaces based on XPS intensities. *Surface and Interface Analysis* **36**, 805-808, doi:10.1002/sia.1769 (2004).

11 Jablonski, A. & Zemek, J. Overlayer thickness determination by XPS using the multiline approach. *Surface and Interface Analysis* **41**, 193-204, doi:https://doi.org/10.1002/sia.3005 (2009).

12 Dreiling, M. J. Quantitative surface measurements of metal oxide powders by X-ray photoelectron spectroscopy (XPS). *Surface Science* **71**, 231-246, doi:https://doi.org/10.1016/0039-6028(78)90330-8 (1978).

13 Ikeno, H. *et al.* Variation of Zr-L2,3 XANES in tetravalent zirconium oxides. *Journal of Physics: Condensed Matter* **25**, 165505, doi:10.1088/0953-8984/25/16/165505 (2013).

14 Park, M. H. *et al.* Ferroelectricity and Antiferroelectricity of Doped Thin HfO2-Based Films. *Advanced Materials* **27**, 1811-1831, doi:https://doi.org/10.1002/adma.201404531 (2015).

15 Williams, E. W. & Bebb, H. B. in *Semiconductors and Semimetals* Vol. 8 (eds R. K. Willardson & Albert C. Beer) 321-392 (Elsevier, 1972).

16 Suzuki, T. & Ogawa, M. Degradation of photoluminescence intensity caused by excitation-enhanced oxidation of GaAs surfaces. *Applied Physics Letters* **31**, 473-475, doi:10.1063/1.89745 (1977).

17 Spirkoska, D. *et al.* Structural and optical properties of high quality zinc-blende/wurtzite GaAs nanowire heterostructures. *Physical Review B* **80**, 245325, doi:10.1103/PhysRevB.80.245325 (2009).

18 Titova, L. V. *et al.* Temperature dependence of photoluminescence from single core-shell GaAs–AlGaAs nanowires. *Applied Physics Letters* **89**, doi:10.1063/1.2364885 (2006).

19 AB, N. P. O. Gerd Binnig – Facts. (2024).

20 Binnig, G., Quate, C. F. & Gerber, C. Atomic Force Microscope. *Physical Review Letters* **56**, 930-933, doi:10.1103/PhysRevLett.56.930 (1986).

21 Corporation, B. *Dimension Icon User Guide*. (Bruker COrporation, 2024).

22 Taylor, D. V. & Damjanovic, D. Piezoelectric properties of rhombohedral Pb(Zr,Ti)O3 thin films with (100), (111), and "random" crystallographic orientation. *Applied Physics Letters* **76**, 1615-1617, doi:10.1063/1.126113 (2000).

23 Balke, N. *et al.* Differentiating Ferroelectric and Nonferroelectric Electromechanical Effects with Scanning Probe Microscopy. *ACS Nano* **9**, 6484-6492, doi:10.1021/acsnano.5b02227 (2015).

24 Kelvin, L. V. Contact electricity of metals. *The London, Edinburgh, and Dublin Philosophical Magazine and Journal of Science* **46**, 82-120, doi:10.1080/14786449808621172 (1898).

25 S. M. Sze, M. K. L. *Semiconductor Devices*. 3rd edn, (John Wiley & Sons, Inc, 2012).

26 Nantite. (Creative Commons Attribution-ShareAlike 2.5 Generic (CC BY-SA 2.5), 2013).

27 Kittel, C. *Introduction to Solid State Physics*. 8th edn, (John Wiley & Sons, Inc, 2005).

28 Huan, T. D., Sharma, V., Rossetti, G. A. & Ramprasad, R. Pathways towards ferroelectricity in hafnia. *Physical Review B* **90**, 064111, doi:10.1103/PhysRevB.90.064111 (2014).

29 Silva, J. P. B. *et al.* Roadmap on ferroelectric hafnia- and zirconia-based materials and devices. *APL Materials* **11**, doi:10.1063/5.0148068 (2023).

30 Sahiner, M. A. *et al.* Identification of structural phases in ferroelectric hafnium zirconium oxide by density-functional-theory-assisted EXAFS analysis. *Applied Physics Letters* **118**, doi:10.1063/5.0038674 (2021).

31 Mao, G.-Q. *et al.* In search of Pca21 phase ferroelectrics. *Journal of Physics: Materials* **6**, 024001, doi:10.1088/2515-7639/acbee2 (2023).

32 Yuan, X. *et al.* Piezoelectricity, Pyroelectricity, and Ferroelectricity in Biomaterials and Biomedical Applications. *Advanced Materials* **36**, 2308726, doi:https://doi.org/10.1002/adma.202308726 (2024).

33 Whatmore, R. W. in *Electronic Materials: From Silicon to Organics* (eds L. S. Miller & J. B. Mullin) 283-290 (Springer US, 1991).

34 Rühle, S. Tabulated values of the Shockley–Queisser limit for single junction solar cells. *Solar Energy* **130**, 139-147, doi:https://doi.org/10.1016/j.solener.2016.02.015 (2016).

35 Shockley, W. & Queisser, H. J. Detailed Balance Limit of Efficiency of p-n Junction Solar Cells. *Journal of Applied Physics* **32**, 510-519, doi:10.1063/1.1736034 (1961).

36 Alcer, D., Tirrito, M., Hrachowina, L. & Borgström, M. T. Vertically Processed GaInP/InP Tandem-Junction Nanowire Solar Cells. *ACS Applied Nano Materials* **7**, 2352-2358, doi:10.1021/acsanm.3c05909 (2024).

37 Espinet-Gonzalez, P. *et al.* Radiation Tolerant Nanowire Array Solar Cells. *ACS Nano* **13**, 12860-12869, doi:10.1021/acsnano.9b05213 (2019).

38 Wacaser, B. A. *et al.* Preferential Interface Nucleation: An Expansion of the VLS Growth Mechanism for Nanowires. *Advanced Materials* **21**, 153-165, doi:https://doi.org/10.1002/adma.200800440 (2009).

39 Mårtensson, T., Borgström, M., Seifert, W., Ohlsson, B. J. & Samuelson, L. Fabrication of individually seeded nanowire arrays by vapour–liquid–solid growth. *Nanotechnology* **14**, 1255, doi:10.1088/0957-4484/14/12/004 (2003).

40 Jiang, N. *et al.* Understanding the true shape of Au-catalyzed GaAs nanowires. *Nano Lett* **14**, 5865-5872, doi:10.1021/nl5027937 (2014).

41 Timm, R. *et al.* Self-cleaning and surface chemical reactions during hafnium dioxide atomic layer deposition on indium arsenide. *Nature Communications* **9**, 1412, doi:10.1038/s41467-018-03855-z (2018).

42 Hinkle, C. L., Vogel, E. M., Ye, P. D. & Wallace, R. M. Interfacial chemistry of oxides on InxGa(1−x)As and implications for MOSFET applications. *Current Opinion in Solid State and Materials Science* **15**, 188-207, doi:https://doi.org/10.1016/j.cossms.2011.04.005 (2011).

43 Luo, J.-D. *et al.* Correlation between ferroelectricity and nitrogen incorporation of undoped hafnium dioxide thin films. *Vacuum* **176**, 109317, doi:https://doi.org/10.1016/j.vacuum.2020.109317 (2020).

44 Naoki Kobayashi, N. K. & Yasuyuki Kobayashi, Y. K. As and P Desorption from III-V Semiconductor Surface in Metalorganic Chemical Vapor Deposition Studied by Surface Photo-Absorption. *Japanese Journal of Applied Physics* **30**, L1699, doi:10.1143/JJAP.30.L1699 (1991).

45 Garcia, V. & Bibes, M. Ferroelectric tunnel junctions for information storage and processing. *Nature Communications* **5**, 4289, doi:10.1038/ncomms5289 (2014).

46 Jia, Y. *et al.* Giant tunnelling electroresistance in atomic-scale ferroelectric tunnel junctions. *Nature Communications* **15**, 693, doi:10.1038/s41467-024-44927-7 (2024).

47 Athle, R. *Ferroelectric Memristors - Materials, Interfaces and Applications*, Lund University, (2024).

48 Saketh Ram, M., Svensson, J. & Wernersson, L.-E. Effects of Interface Oxidation on Noise Properties and Performance in III–V Vertical Nanowire Memristors. *ACS Applied Materials & Interfaces* **15**, 19085-19091, doi:10.1021/acsami.2c21669 (2023).

49 Carboni, R. & Ielmini, D. Stochastic Memory Devices for Security and Computing. *Advanced Electronic Materials* **5**, 1900198, doi:https://doi.org/10.1002/aelm.201900198 (2019).

50 TheNoise. (Creative Commons Attribution-ShareAlike 2.5 Generic (CC BY-SA 2.5), 2007).

51 Yao, M. *et al.* GaAs Nanowire Array Solar Cells with Axial p–i–n Junctions. *Nano Letters* **14**, 3293-3303, doi:10.1021/nl500704r (2014).

Printed by Media-Tryck, Lund 2024 NORDIC SWAN ECOLABEL 3041 0903

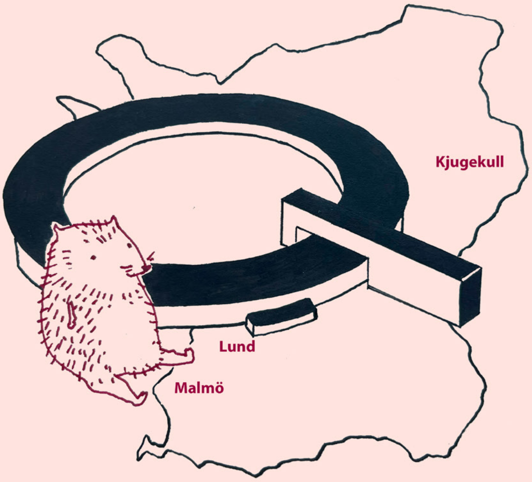

LUND
UNIVERSITY

Department of Physics
Faculty of Science

ISBN 978-91-8039-980-7